Reference Material 8634
Ethylene Tetrafluoroethylene for Particle Size Distribution and Morphology

Dean Ripple
Srivalli Telikepalli
Kristen Steffens
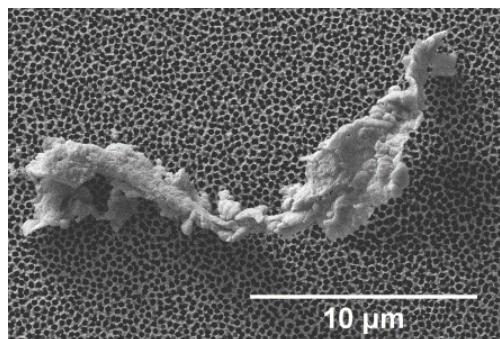Michael Carrier
Christopher Montgomery
Nicholas Ritchie
Z. Q. John Lu

NIST Special Publication 260-193

Reference Material 8634
Ethylene Tetrafluoroethylene for Particle Size Distribution and Morphology

Dean Ripple
Srivalli Telikepalli
Kristen Steffens
Michael Carrier
Christopher Montgomery
Biomolecular Measurement Division
Material Measurement Laboratory

Nicholas Ritchie
Materials Measurement Science Division
Material Measurement Laboratory

Z. Q. John Lu
Statistical Engineering Division
Information Technology Laboratory

May 2019

U.S. Department of Commerce
Wilbur L. Ross, Jr., Secretary

National Institute of Standards and Technology
Walter Copan, NIST Director and Undersecretary of Commerce for Standards and Technology

Abstract

Reference Material (RM) 8634 is a NIST particle standard produced from abraded ethylene tetrafluoroethylene (ETFE), a chemically inert polymer, that will help standardize and allow more accurate monitoring of subvisible proteinaceous particles in biotherapeutics. These ETFE particles resemble proteinaceous particles in biotherapeutics because they are translucent, with a refractive index similar to that of proteinaceous particles, and have irregular morphology. RM 8634 has reference values for particle size distribution (PSD), in the range of (1 to 30) µm, and morphology (aspect ratio, compactness, ellipse ratio). The PSD values were obtained using flow imaging (FI), an in-house-devised stop-flow microscope (SFM), and a static optical microscopy technique. For morphological assessment of the particles, SFM, scanning electron microscopy (SEM), and static optical microscopy techniques were employed. All techniques employed were highly characterized for instrument biases and appropriate corrections were made; rigorous statistical analysis of the data was performed to obtain the reference values. This document briefly describes the preparation of the RM, data collection, data analysis, data compilation, and reference value assignment. Detailed procedures of how the analyst can use this RM to obtain PSD and morphology information, qualify instruments, reduce variability, and correct for instrument biases are presented. The document also describes how the analyst will be able to apply corrections, obtained from RM analysis, to protein-like samples to obtain more accurate PSD and morphology information than if the correction is based solely on polystyrene microspheres. Such a standard is the first-of-its-kind available to the industry. We envision that RM 8634 will drive industrial collaboration to better characterize and, in turn, understand the implications of proteinaceous particles in biotherapeutics.

Keywords

Table of Contents

List of Tables

List of Figures

Glossary

Aspect ratio, f_{asp}—ratio of minimum and maximum Feret diameters

CDF, Center Distance Finding—a method of sizing spheres by measuring the distance between centers in an image

Circularity, f_{cir}—ratio of particle perimeter to the perimeter of the circle with equivalent circular diameter

Compactness, f_{comp}—ratio of equivalent circular diameter to the maximum Feret diameter

Complementary cumulative distribution, $N(d)$—number of particles per milliliter greater than or equal to the specified diameter

Coverage factor, k—a multiplier relating the expanded uncertainty U to the combined standard uncertainty (i.e., estimated standard deviation) u_c by the equation $U = ku_c$

DIUF—de-ionized ultra-filtered water

Equivalent circular diameter, d—diameter of the circle with the same area as the filled area of the particle, after correction for optical resolution effects

Ellipse ratio, f_{ell}—ratio of minor and major axes (L_{min} and L_{maj}) of the ellipse with the same area and ratio of second moments as the measured particle

ESDM—experimental standard deviation of the mean

ETFE—ethylene tetrafluoroethylene

Feret diameter, F—distance between two parallel planes touching a particle border but not intruding into the particle interior

FI—flow imaging, a variant of dynamic imaging in which a sample flows through a cell while images of the sample are acquired and analyzed automatically. In this document, FI refers to the particular instrument used in this study.

IgG—immunoglobulin G

LO—light obscuration, a technique that measures the decrease in light intensity as a particle passes through a light beam and converts that into the apparent size of the particle

Measured diameter, d_m—diameter of the circle with the same area as the filled area of the particle prior to correction for known biases

PC—Palmer chamber, a microscope slide with a well-defined chamber volume that allows one to manually size and count the number of particles in the chamber volume.

PEEK—polyether ether ketone

PETG—polyethylene terephthalate glycol

PFA—perfluoroalkoxy

PMMA—poly(methyl methacrylate)

PSD—particle size distribution

PSL—polystyrene latex

1

PVDF—polyvinylidene fluoride

RM—reference material

SD—standard deviation

SEM—scanning electron microscopy

SFM—stop-flow microscope, a variant of dynamic imaging in which a sample is injected into the cell, particles are allowed to settle, and images are acquired and analyzed automatically. In this document, SFM refers to the particular in-house designed instrument used in this study.

1. **Introduction**

Reference Material RM 8634 is composed of particles prepared from ethylene tetrafluoroethylene (ETFE), which are irregular in morphology, highly transparent, and have a refractive index n of ≈ 1.4. These physical properties of ETFE resemble those of proteinaceous particles in biotherapeutics. Hence ETFE particles are an excellent candidate to become a standard to more accurately characterize translucent and unstable subvisible proteinaceous particles. This standard will allow for more repeatable and accurate monitoring of subvisible proteinaceous particles in biotherapeutics. The first five sections of this document describe the fabrication and characterization of the ETFE particle solution comprising RM 8634. Users interested in instructions for use of RM 8634 may wish to begin at Section 6.

Briefly, to prepare the particles, the ETFE was first abraded against a diamond abrasive disc in a well containing a surfactant solution, filtered, settled, and harvested (as described in Section 2). The final suspension containing the particles of interest, packaged as RM 8634, was characterized for particle size distribution (PSD) and various morphological parameters (characterizing the non-spherical nature of the particles). The reported values for this RM are the number, or particle size, distribution (expressed in number of particles per milliliter, N, greater than a specified equivalent circular diameter, d) and several morphological parameters (aspect ratio, compactness, and ellipse ratio) for a range in d of 1 µm to 30 µm.

The PSD was measured using three instruments: 1) a commercial dynamic imaging instrument (FI) which captured images of particles flowing through a flow cell; 2) a stop-flow microscope (SFM) which flowed suspension through a horizontal cell, allowing the particles to settle before imaging them, and 3) a manually filled cell (Palmer Chamber, PC) with equivalent optics as used with the SFM measurement. Sections 3 and 5 present the methods and results of these PSD measurement methods. Appendix B summarizes uncertainties and biases associated with these measurements. Additionally, diameter corrections were applied by modifying a commercial upright optical microscope to mimic the optics of the FI, SFM, and PC measurement methods. Individual ETFE particles, immobilized in gelatin, were measured at a low-resolution configuration (mimicking the configuration of the PSD measurement techniques) and in a high-resolution configuration. From a set of these low-resolution/high-resolution images, a correlation was developed to give a correction of the low-resolution diameters to the apparent true diameter (see Appendix

A). To apply this correlation, we mathematically determined what reported diameter (from FI, SFM, or PC) corresponded to the actual particle diameter that we wished to report in the Report of Investigation. The diameters are traceable to the International System of Units (SI) through a calibrated stage micrometer [1] that was used to either directly calibrate the pixel size of measured images or to calibrate the diameters of monodisperse microspheres. The particle number concentrations are traceable to suspensions of polystyrene microspheres that have number concentration measurements determined using techniques that we have developed [2].

The particle morphology (aspect ratio, compactness, and ellipse ratio) was measured by three methods: 1) the same SFM as described above, 2) the same PC measurements as described above, and 3) scanning electron microscope (SEM) measurements of particles captured on porous alumina filters.   The methods used for these techniques and results for determining the morphological parameters are described in Sections 4 and 5, respectively; the associated uncertainties are detailed in Appendix C. Traceability for morphology measurements was assured by calibrating pixel sizes of the digital images and by validating software using artificial images of known morphology.

To obtain the most accurate PSD and morphology data possible, corrections were applied for known instrument biases. The reported measurements are intended to be accurate representations of the PSD and morphological parameters independent of the particular instruments used for assigning the reference values. Appendices B and C report measurement uncertainties and known biases.

This document also provides detailed information regarding the sample and how it can be used by the analyst (Sections 6 to 11). Section 6 gives important guidelines to the handling of RM 8634. Methods to correct reported diameters to reduce variability among instruments using RM 8634 are described in Section 7. Section 8 gives a method for determining the PSD for an ETFE working standard using RM 8634. The ETFE particles can be diluted into various concentrations of glycerol-water to mimic the optical properties of very translucent proteinaceous particles; this procedure is described in Section 9. Section 10 describes how the RM 8634 can be analyzed with light obscuration (LO) counters. Section 11 provides general guidelines for accurate measurement of high-density particles, including those in RM 8634.

RM 8634 can be used for system suitability checks and qualification of instruments used to monitor subvisible proteinaceous particles in biotherapeutics. It can be used to determine instrument biases for size, concentration, and morphological parameters of proteinaceous particles. The bias correction that will be obtained after analysis of the RM on an optically-based particle characterization instrument can be applied to all protein-like samples to get truer PSD and morphology information than if the correction is based on microspheres. Overall, having a well-characterized standard that is readily available will support better characterization and, in turn, understanding of the implications of proteinaceous particles in biotherapeutics.

3

2. Fabrication of RM 8634

2.1. Background

ETFE polymer has many desirable properties that make it a good candidate for a reference material. The plastic is rugged, chemically inert and mechanically strong. It has a refractive index close to 1.4, similar to that of protein [3,4], and the material can be made mechanically into irregular, translucent particles. Particles can be generated easily by abrading ETFE against a diamond disc in a well containing a surfactant solution; the particles can be produced in a broad size range, from nanometers to many micrometers in size.

Figure 1 below shows the starting material for preparing the particles: the ETFE tubing as well as the in-house devised ETFE abrader consisting of a motor that grinds a mass-loaded ETFE tube against the diamond abrasive disc in a well containing diluent. Figure 2 displays the similarity in appearance of the ETFE particles to typical proteinaceous particles from an immunoglobulin (IgG) molecule by two methods.

Particle preparation, vial preparation, and vial filling were all conducted at the National Institute of Standards and Technology (NIST). RM 8634 provides values for PSD and morphology. The RM material had to meet the following pre-established criteria:

- aqueous suspension of ETFE particles with a morphology representative of actual protein particles;
- particle size range from <1 µm to ≈ 50 µm;
- suspension free of non-ETFE particles or other contamination to the extent possible;
- $N(1\,\mu m)$ sufficiently low to allow direct use in commercial light obscuration (LO) instruments and $N(25\,\mu m) > 400\ mL^{-1}$ to enable good counting statistics for $d = 25\,\mu m$;
- shelf life of three years.
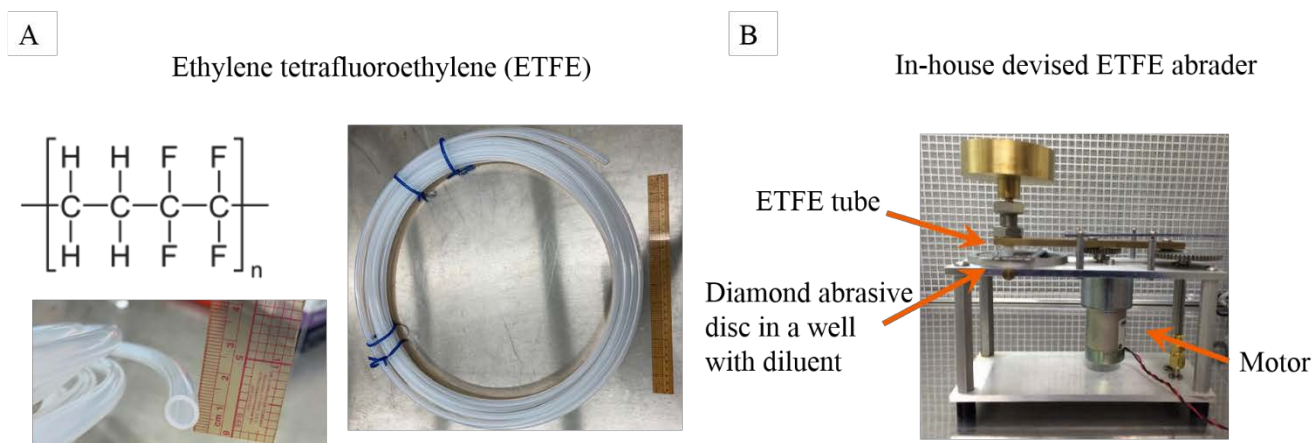
Figure 1.   The ETFE tubing shown in A) is used to produce ETFE particles using the B) in-house devised abrader utilizing a diamond abrasive disc.

4

Flow Imaging: Morphology of IgG vs. ETFE Particles

SEM Images of ETFE Particles

IgG (30 µm to 40 µm)

ETFE (30 µm to 40 µm)

Particles captured on anodized alumina filters.
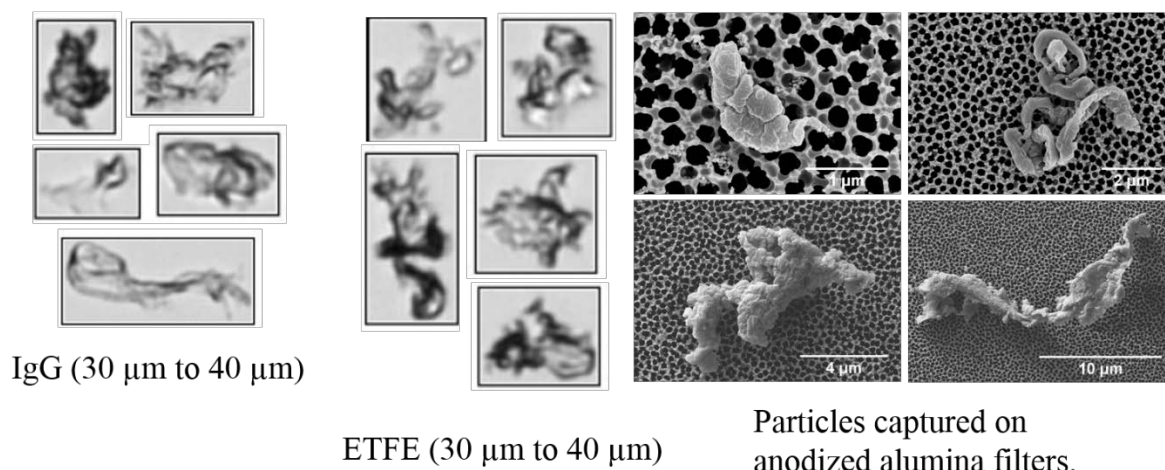
Figure 2. The morphology of representative IgG particles and ETFE are shown by images obtained by A) flow imaging and B) scanning electron microscopy.

2.2. Formulation

The ETFE particles are suspended in a solution of 0.02% mass concentration Triton X-100 (Sigma-Aldrich, St. Louis, MO) and 0.02% mass concentration sodium azide (Ricca Chemical Company, Arlington, TX) in 18 MΩ·cm deionized ultra-filtered water (DIUF). (This solution is hereafter labeled diluent.) All diluent was prepared in laminar flow hoods using clean, calibrated glassware, balances, and pipettes. The diluent was filtered through 0.22 µm polyvinylidene fluoride (PVDF) membrane vacuum filtration units (Stericup and Steritop, Millipore, Burlington, MA). Prior to use, filters were washed and particle concentration was measured to be low (N(1 µm)< 100 mL^{-1}) using an FI instrument (ProteinSimple DPA 4200, San Jose, CA).

2.3. Preparation of ETFE Particles and Filling of Vials

The ETFE particles were created by abrading pieces of ETFE tubing (nominal 0.95 cm outer diameter and 0.71 cm inner diameter and supplied by Saint Gobain (Mickleton, New Jersey; resin lot 1402pf8817)), as shown in Figure 1A. All equipment used for this process was extensively cleaned and was verified to ensure that it generated a minimal number of particles relative to the particle concentration in the RM. The abrasion apparatus, shown in Figure 1B, was custom built at NIST. A motor with an integral gear head (specified for 7 revolutions per minute (0.7 rad/s) at 1.0 N·m torque) drove a four-point linkage. A sleeve comprised of a hollow bolt and lock nut mounted at the end of the linkage held the ETFE tube; a 1.00 kg mass forced the ETFE down on a diamond abrasive disc. The linkage converted the motor motion into an elliptical path of the ETFE tube across the disc face. The

5

nickel-bonded diamond abrasive discs with 125 µm grit size were placed at the bottom of machined, anodized aluminum wells that could hold up to 15 mL of diluent.

To prepare ETFE particles, multiple lengths of the ETFE tubing were cut to approximately 4 cm in length, with one end of the tubing cut at a ≈ 20° angle from a face perpendicular to the tube axis. The angled end of the tubing pressed against the diamond, 10 mL of diluent was added to the well, and the abrader set to run for 10 min at 38 elliptical cycles per minute. Only a fraction of the tubing was abraded so as to not exceed the tapered portion of the tubing. Particles were washed off the diamond disc and transferred to a clean polyethylene terephthalate glycol (PETG) collection vial. This process was repeated multiple times to collect the desired volume of ETFE suspension.

After collection, the vial was shaken for 20 s to disentangle particles and allowed to sit in the laminar hood for 1 h to reduce the foam. Particles larger than 50 µm were filtered out by passage through a prewashed nylon screen with 53 µm openings. Approximately 50 mL of the filtered solution settled for 8 min to increase the relative concentration of the larger particles at the bottom. A pipette was then used to gently pull out all but the lowest 10 mL of diluent. The bottom 10 mL (which should contain more of the larger particles) was removed and stored in another clean labeled PETG container. This process was repeated to obtain ≈ 80 mL of the "bottom" settled ETFE solution. To assess the PSD, measurements were then taken on diluted samples of the retained solution with an FI system. As a figure of merit for the relative concentration of larger particles, we used

$$R_{1,20} = \frac{N(d = 1 \text{ µm})}{N(d = 20 \text{ µm})} \quad .$$

(1

The ETFE solution was acceptable for use provided $R_{1,20} < 30$.

The concentrated ETFE solution was diluted to the desired number concentration prior to filling into pre-cleaned perfluoroalkoxy (PFA) vials of nominal 22 mL volume (Savillex, MN). As part of the cleaning, the PFA vials were soaked in a solution of hot Triton X-100; adsorption of Triton X-100 lubricated the vial threads. The ETFE suspension was delivered into the PFA vials (verified clean from light obscuration measurements) from a 20 L PVDF tank equipped with a stirrer, a sampling tube with a Teflon valve that entered the bottom of the tank and extended 10.5 cm into the tank, a fill opening on the lid, and a silica-glass sheath mounted to the lid to allow insertion of an ultraviolet (UV) sterilization bulb. Four stainless steel baffles attached to the lid reduced vortexing and promoted thorough mixing [5]. The tank and associated parts were extensively cleaned before adding any of the diluent or ETFE particle suspension and checked for low particle content. The tank was filled with appropriate volumes of diluent and the "bottom" settled ETFE, as described in the previous section, and verified on the FI instrument to have the desired particle concentration. The tank and contents were sterilized prior to the fill using a UV bulb placed in a silica glass sheath (TM13, Atlantic Ultraviolet Corporation, Hauppauge, NY). Based on a UV measurement of bulb output, we sterilized for three 5 s exposures, separated by ≈ 10 s for the tank liquid to recirculate.

6

Vials were filled in assembly line fashion, under nominally aseptic conditions from a continuously flowing stream through the tube at the bottom of the tank while the tank was continuously stirred. As the liquid level dropped during the fill, the stirring speed was incrementally reduced to ensure no foam was being generated. Five hundred vials were filled with approximately 20 mL solution each, given an initial tightening and were tightened further the next day for a more secure seating of the caps to the vials.

3. Particle Size Distribution of RM 8634

3.1. Overview

The particle size distribution (PSD) is reported as the number of particles per milliliter greater than or equal to the specified diameter, $N(d)$, which is also termed the complementary cumulative number distribution, for d from 1 µm to ≈ 50 µm. The PSD was measured using three instruments: 1) a commercial dynamic imaging instrument (FI) that captures images of particles flowing through a flow cell; 2) a stop-flow microscope (SFM) that flows suspension through a horizontal cell, stops the flow, allows the particles to settle, and acquires images of the settled particles; and 3) a manually filled cell (using a Palmer Chamber, PC) with equivalent optics as used with the SFM. For these measurements approximately 20 ETFE vials from the fill were chosen for assessment of the PSD and morphology (morphology assessment described in Section 4). All optical microscopes are subject to errors due to blurring of the images from optical diffraction, and these effects can be difficult to assess for irregular particles such as ETFE. Appendix A describes the methods used to correct for these effects. Appendix B summarizes the uncertainties and known biases of all three methods used to determine the PSD.

Before analyzing the RM sample, it was necessary to determine the size and number concentration accuracy of some of the methods using microsphere standards. For determining number concentration, the methods of Ripple and DeRose [2] were used to find the number concentration of several microsphere lots that were subsequently used to calibrate the FI, SFM, and PC sample cells. For determining diameter accuracy, two methods were used. In the first method, microsphere diameters were measured by the method of Center Distance Finding (CDF) [6], in which the centers of dried samples of poly(methyl methacrylate) (PMMA) microspheres were measured using a calibrated optical microscope and a 10× or a 40× objective (depending on the size of the microspheres) with Köhler illumination. In the second method, a more direct measurement of the pixel size was obtained for microscopic techniques (SFM and PC), where the pixel size of the camera images was obtained using a calibrated stage micrometer with nominal 25 µm ruling spacings [1]. Image pixel sizes were obtained for each microscope objective used. A direct measurement of the pixel size for the DPA 4200 FI instrument was performed using a small section from a plastic Ronchi ruling taped to the cell holder in such a way that the plane of the plastic film was slightly tilted and passed through the focal plane of the DPA 4200. The same area of the film that was imaged by the DPA 4200 was imaged in a calibrated upright optical microscope to determine the pitch of the Ronchi film.

3.2. **Flow Imaging**

Commercial flow imaging instruments are capable of rapid measurement and analysis of multiple samples and are thus an excellent choice for PSD measurements to assess the homogeneity among the vials and measurement repeatability within single vials of the RM 8634 lot. We conducted multiple independent experiments to qualify our FI instrument and validate our measurement method prior to measurement of the RM vial lot.

A Micro-Flow Imaging DPA4200 flow imaging (FI) instrument (Set Point 3, 4× objective, 100 µm thick flow cell), MVSS V. 2, and MVAS 1.4 software (ProteinSimple, San Jose, CA) were used for acquiring, exporting, and analyzing data. Samples were loaded using Neptune 1 mL barrier pipette tips (San Diego, CA), and low protein-binding pipette tips (Eppendorf, Germany) were used for cleaning the tubing and flow cell between runs. Prior to running any samples on the flow imaging instrument (FI), the instrument was cleaned and maintained according to manufacturer's recommendations. All samples were run according to the method described below for rapidly settling particles (see Section 11).

3.2.1. **Experiments and Results**

The shape of a polydisperse PSD can be altered by errors in either particle count or particle size. Additionally, lot homogeneity and stability of the reference material were evaluated to understand the properties of the batch as well as the repeatability of the measurements. Not all experiments conducted are discussed below as they did not contribute significantly to the uncertainty in the measurements. The results of the experiments were used to optimize the method and to generate corrections or uncertainty values for both particle size and concentration (see Appendix B for tabulated values).

3.2.1.1. **Concentration Biases**

To assess concentration biases, measurements were performed pertaining to both the adsorption of ETFE particles on the tubing walls, flow cell, or pipette tips and to the effectiveness of water or diluent to sweep off ETFE between runs. It was observed that large ETFE particles increase in number concentration at the end of the run as the meniscus passes through the tubing, likely due to the meniscus sweeping particles off the tubing walls. Multiple runs were performed where the particles could be imaged all the way through passage of the meniscus through the cell. To quantify this error, runs were begun with smaller than usual ETFE load, followed by diluent added on top of the vapor gap that formed and the run completed. Compilation of particle images versus time were inspected to determine the quantity of particles detected after the normal ending point of the run. A small increase in concentration was observed near the end of the run, especially for particles $\geq 10\ \mu m$.

The cell thickness can also impact the number concentrations obtained since the number of particles detected per image is proportional to the actual thickness of the cell. The flow cell used for both FI and for the SFM (described below) is reported to be nominally 100 µm thick by the manufacturer. A solution of 4 µm polystyrene microspheres was measured on a highly characterized light obscuration (LO) instrument and on FI. Correction factors, described by Ripple and De Rose [2], were applied to the LO concentration measurements to obtain microsphere number concentrations traceable to the International System of Units

(SI). The minor difference observed between the FI experimental values for microsphere number concentration and absolute values (the corrected LO results) was attributed to a cell thickness slightly different than the 100 µm nominal thickness. In all cases tested, the actual cell constant thickness agreed with the nominal thickness to within manufacturer's specifications.

Lot homogeneity and stability of RM 8634 were evaluated primarily by the FI method. For this experiment, 10 vials were chosen to span the entire fill process from vial 1 to vial 500, which roughly corresponds to the time they were collected (lower numbered vials were collected earlier than higher numbered vials). The vials were analyzed in a randomized order on the FI instrument by two analysts on two days. Analysis of the homogeneity data demonstrated that the lot homogeneity was a small contributor to the overall uncertainty.

The shelf-life stability and shipping stability of the vials were assessed by placing them at (2 to 8) °C and 23 °C for up to four months, and shipping them cross country to another NIST facility, respectively. Additional RM vials were exposed to potential harsh environmental conditions such as storage at 40 °C for three days and frozen at –20 °C (and underwent 1 freeze/thaw, labeled 1 FT).   There was virtually no change in the concentration when stored at (2 to 8) °C and 23 °C ($p > 0.05$ for all size bins using Student t-test); the FI results for the stability-test vials were consistent with the homogeneity measurements. Negligible change in particle concentrations was observed before and after shipping in all size ranges ($p > 0.05$) except for a marginal statistical change observed in bin ≥ 7 µm. For the samples subjected to 1 FT at –20 °C, there were significant changes in particle concentrations (compared to the sample that did not undergo 1 FT) observed for particles below 15 µm in size ($p < 0.01$ for all bins ≤ 10 µm and $p < 0.05$ for particles in the bin ≤ 15 µm). The samples subjected to 40 °C for three days did not show a significant difference in particle concentration for particles larger than 5 µm, compared to the time $T = 0$ data ($p > 0.05$). However, particles in the ≥ 2 µm and ≥ 3 µm bins exhibited a small (≈ 2 % of the number concentration, N), marginally statistically significant increase in particle concentration as compared to the $T = 0$ data ($p < 0.05$.)

3.2.1.2. Diameter Biases

For diameter biases, the most important factor is correction for diffraction effects resulting from the limited optical resolution of the imaging system. We have corrected these effects, using a correlation between high and low-resolution optical images conducted on a separate optical microscope (See Appendix A).

We have also looked at the variance in the FI diameter reading to obtain the likely deviation of the "true" PSD from the measured PSD using cumulative distribution of several runs and a mathematical function generated for the average PSD. Artificial data sets were created in which 150 000 particles were randomly selected in accordance with the average PSD. The diameter of each particle was randomly varied using a Gaussian probability distribution. A histogram was obtained from both the original data set and the set with Gaussian variation to compile a Monte Carlo simulation. The results of these simulations demonstrated that these convolution effects, which can result in mis-assignment of particle diameter, are generally small, less than 5 % across all reported FI size ranges, with the maximum effect occurring for $d \geq 5$ µm and $d \geq 7$ µm.

9

3.2.2. Data Analysis

Data obtained by the FI was exported to spreadsheet format for further analysis to assess for any errors in PSD due to stuck particles and to correct for cell thickness, or incorrect counting/sizing of particles that appear on or near the edge of the frame.

To remove stuck particles, a Python 3.6 script [7] extracted raw data from exported FI files and applied a filter to remove stuck particles to prevent over-counting. The output of the script was imported to an Excel template that then rejected particles with a center of mass within a certain distance from the image edge, adjusted for sample dilution from the water-priming step, and generated an $N(d)$ histogram.

The FI software can be configured to either accept or reject particles that intersect an edge. Large particles are more likely to intersect an edge, and edge particles have an incorrect particle size and morphology. To assess the impact of accepting/rejecting edge particles on the PSD, we chose to use a measurement frame approach [8], in which the only particles counted are those with a center of mass within a rectangle (termed the measurement frame, as shown in Figure 3) inscribed within the total field of view. There are hydrodynamic effects that can alter the particle distribution near flow-cell walls [9]; however, we found that implementing a measurement frame to exclude particles near the flow-cell walls introduced a greater uncertainty by limiting the flow-cell cross section that was probed than by mis-sizing edge particles. Consequently, particles whose centers of mass were within 30 pixels from the left and right edges were discarded, as shown in Figure 3.

The distribution of particles across the flow-cell width is not uniform for larger size particles, as shown in Figure 4. In our particular FI instrument, one side of the flow cell was very close to the edge of the image, but the opposite edge of the image did not extend to the flow-cell wall. The particle counts expected across the full flow-cell width, from integration of the observed profile combined with the width of the unimaged portion of the flow cell, was compared to the particle counts obtained in the FI measurement frame. The ratio of these counts is equal to the correction factor for edge particles.
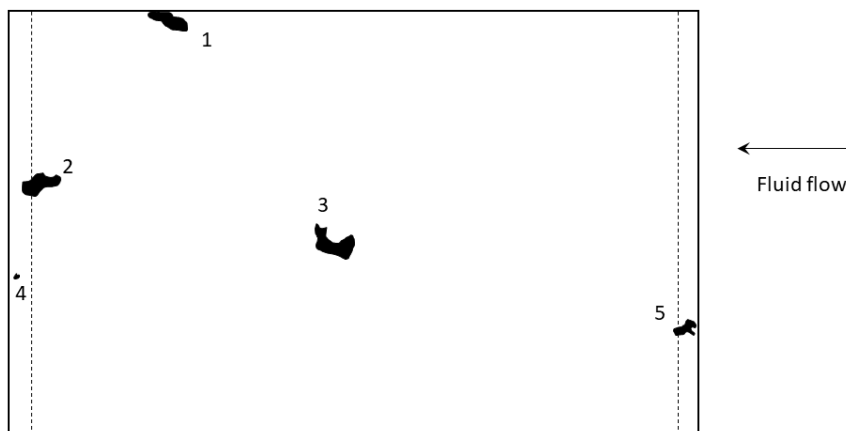
Figure 3. Measurement frame for flow imaging; particles 1, 2 and 3 are included in the count, while particles 4, and 5 are excluded. The flow cell walls are located at the top and bottom of the image (which is rotated relative to the physical orientation of the flow cell).

10
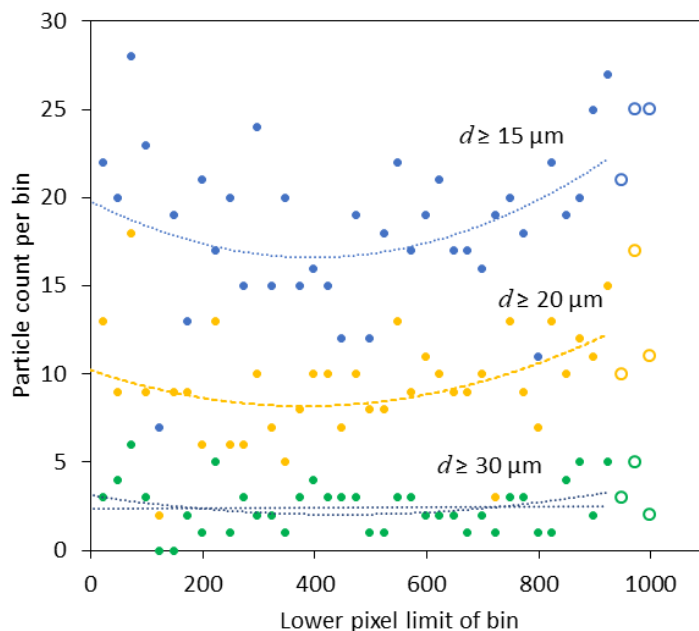
Figure 4. Non-uniform particle distributions across the width of the FI flow cell. Open symbols show the pixel range used to estimate the number concentration at the one side of the cell that had a significant unimaged strip.

3.2.3. Uncertainty of FI PSD Measurements

For the FI measurements, the uncertainty component for the diameter is the dominant component for all size limits. The method of correcting the diameter is described below in Appendix A. Briefly, an upright optical microscope with a modified-numerical aperture microscope objective was used to mimic the optical response of the FI and to generate diameter corrections for the FI.

As discussed in Appendix A, this diameter correction and its related uncertainty did not account for asymmetries in the FI ETFE images for sizes smaller than 7 µm. Since this is currently being investigated, we only include FI data for sizes ≥ 7 µm in the reference value assignment. Images at smaller diameters have an asymmetry such that out-of-focus particles are identified only as "arcs" instead of filled particles, resulting in significant undersizing of the particles. We quantified this effect by determining the vector from the binary-image centroid to the middle of the maximum Feret's diameter chord. For randomly oriented images, or for images randomly flipped about the *x*-axis (parallel to the flow path), the *y* component of this vector should be statistically indistinguishable from zero. Figure 5 shows that there is a significant asymmetry for diameters below 7 µm.

11
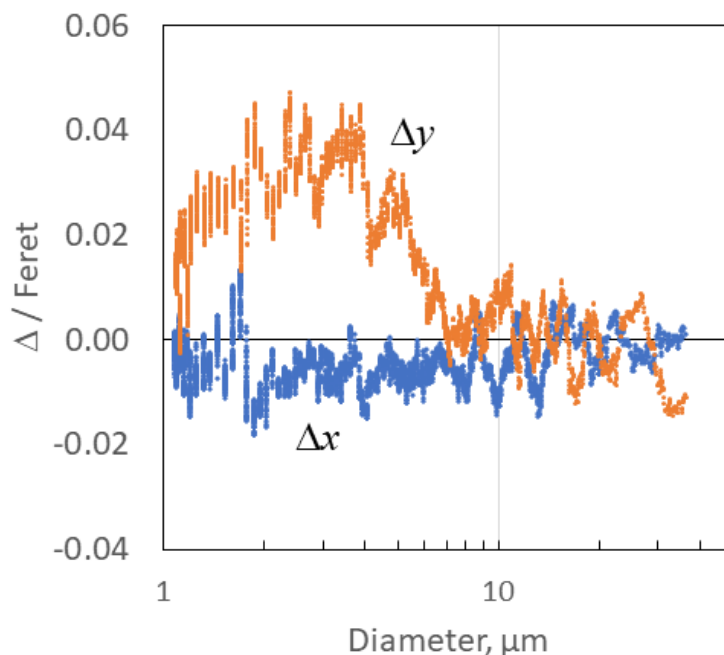
Figure 5. FI image asymmetry, as measured by *x* and *y* components of the vector from the centroid to the middle of the maximum Feret's diameter chord.

3.3. Stop Flow Microscope

FI requires an optical depth of field comparable to the flow cell thickness, and the instrument that we used restricts the numerical aperture of its objective to achieve this. A small numerical aperture reduces the optical resolution, however. To overcome this constraint, we built a custom SFM in which the sample was pulled from a stirred vial through an FI flow cell that was in a horizontal position. After a set of prescribed flushes, the flow stopped and the ETFE particles settled to the bottom window of the flow cell. The focal plane of the instrument was set at a position that maximized the contrast of the smallest particles. Once settled, all particles were close to the same focal plane, and an optical system with much better resolution could be used. Because the sample throughput was low, we used ETFE samples 2.5× and 5× more concentrated (gravimetrically prepared from the same concentrated ETFE stock that was used to make the RM lot) than the actual RM vial lot to increase the number of measured particles. Multiple FI measurements of these concentrated lots confirmed the concentration factors of the SFM samples. The higher concentration SFM samples were also useful in determining the linearity of the SFM and FI.

3.3.1. Instrument Setup & Sample Acquisition

The basis of the SFM is a customized Zeiss Axiovert S100TV inverted microscope, a stirred sample vial, a commercial FI flow cell, and a syringe pump that draws sample through the flow cell. A custom mount on the microscope stage supported a horizontally placed ProteinSimple uncoated cell, nominally 100 µm thick, 1.6 mm wide, and a 7 mL PFA vial (the sample reservoir) with a hole drilled into the cap for sample introduction and a hole in the vial side to mount the entrance tube of the ProteinSimple cell. The sample vial contained a small custom-made stirring paddle attached to a stir controller (Brightwell Stir Controller) set to 84 rad/s (800 revolutions per minute), as well as three vertical baffles that improved the

12

mixing of the ETFE solution. A disk-shaped particle shield, 3.4 cm in diameter, was placed on the stir shaft just below where the stir rod connects with the stir controller to reduce extrinsic particle intrusion into the sample vial. A computer-controlled relay turned the stirrer off and on. A syringe pump pulled cleaning fluids and the sample through the flow cell. Polyether ether ketone (PEEK) tubing connected the flow cell to a 10 mL glass syringe. The use of PEEK and glass materials, combined with thermal insulation of both the tubing and the syringe, minimized liquid flow due to thermal expansion or contraction. The SFM was fully automated, with software written in LabView 2013 (National Instruments, Austin, TX). The microscope was equipped with a 10× Neofluor/0.30NA objective, a Zeiss long working distance condenser for Axiovert inverted microscopes (Oberkochen, Germany), and an Andor Zyla 5.5 sCMOS camera (Oxford Instruments, Abingdon, UK) mounted to the microscope with a 1× coupler. The key camera parameter for low-noise brightfield images is a large well depth (the maximum number of electrons that a single pixel can store), since the noise in this imaging mode is proportional to $1/n_e^{1/2}$, where n_e is the electron well depth. The flow cell was illuminated with a blue LED illuminator with wavelength 455 nm (Model M455L3-C2, ThorLabs, Newton, NJ, USA); optimal intensity stability was obtained by adding a 1.0 optical density neutral density filter.

The fluidic system was cleaned by flushing with 0.02% mass concentration Triton X-100 followed by flushing with (20 to 30) mL of DIUF. The system was then checked with water and diluent blanks on a regular basis to assess the cleanliness of the system. The tilt of the flow-cell holder was adjusted so that 1 µm silica microspheres were in focus throughout the camera image. The condenser was set to give Köhler illumination. Pixel size was calibrated by acquiring images of a calibrated stage micrometer. To calibrate the flow-cell thickness, the cell was dismounted at the end of all runs, installed in the FI instrument, and calibrated as described above for the FI (Section 3.2.1.1).

With a 10× objective in optimal focus, a 1 µm ETFE particle is nearly transparent because of the low refractive index difference between ETFE and water. Image stacks of ETFE obtained at different flow-cell heights relative to the focal plane showed that small particles had optimal contrast while still being acceptably in focus with the focal plane set to be 6 µm farther from the objective than the focal plane corresponding to ETFE at its most transparent state. Investigation of these image stacks also showed that the position of the "most-transparent state" could be readily resolved with 2 µm resolution. All ETFE runs were conducted with the 6 µm offset to the focal plane.

Initial SFM runs revealed difficulties in fully flushing settled particles from the flow cell. Small particles are the most difficult to flush out, since larger particles extend into the flow field where larger fluid velocities can flush them out [10,11]. Insufficient flushing led to a slow rise in particle counts with successive images. To mitigate this effect, a large 200 µL flush was performed at the beginning of the experiment and after every 10 images. With the inclusion of the 200 µL flush, particle buildup in intervening images appeared to be small for a sequence of three 10 µL flush volumes and negligible for a sequence of three 20 µL flush volumes between individual images. The settling time was calculated on the basis of a 1 µm ETFE particle settling the full 100 µm depth of the flow cell. Based on these observations, we conducted a full factorial experiment with two replicates to investigate the effect of

particle concentration (2.5× and 5× of RM vial concentration), settling time (4 min and 6 min), and flush volume (3×10 µL and 3×20 µL) on the PSD.

For analysis, 7.5 mL of the sample was pipetted carefully through the reservoir opening. The stirrer was quickly placed into the reservoir to ensure no settling occurred and the sample run was initiated promptly. The 200 µL flush, performed at the beginning of the run and every 10 images afterward, consisted of the following steps: 1) mix the sample for 20 s; 2) wait 20 s; 3) flush 200 µL of sample; 4) wait 100 s. The acquisition cycle for each image is as follows: 1) spin 20 s; 2) wait 20 s; 3) flush 3 pulses of 10 or 20 µL of the sample; 4) acquire background; 5) let the particles settle for (4 or 6) min; 6) acquire image. These steps were repeated to collect the required number of images. Each run lasted (6 to 8) h to accumulate 50 to 100 images, depending on the flush volume. Diluent runs conducted between ETFE sample runs confirmed the system cleanliness. For the diluent runs, 10 µL pulses and 4 min wait times were used and were manually terminated, after ≈ 5 images were collected.

3.3.2. Experiments and Results
Several experimental parameters can influence the PSD results obtained from the SFM such as sedimentation of the particles, evaporation of the sample over the course of a run, and differences in flow cell thickness.

The runs can take many hours to complete, and during this time the sample could evaporate and result in incorrect PSD determination. Fortunately, evaporation, up to 20 h, was found to be negligible. For the RM samples that were run only with the 20 µL flush volume data used, the evaporation rate ranged from 1.2 % to 1.6 % over the span of an 8 h run.

If particles accumulated in the inlet tube and were then swept partially out to the flow cell, or if the particle settling is incomplete, particle counts could be incorrect. These effects depend on instrumental parameters such as the flush volume and the wait time between each image. Since runs were several hours long, the number of particles measured in the first half of the run was compared to the number of particles measured during the last half of the run. The flush volume had the strongest effect on the concentration measured ($p < 0.01$). The runs performed with 10 µL pulses showed inconsistencies in the PSD with the difference being more prevalent for particles < 15 µm. We surmise that whenever the flow stops, particles settled towards the bottom of the inlet tube and the flow cell. When the flow is initiated, there is a critical velocity necessary to lift the particles off the surface [10,11]. Estimates of this velocity for the inlet tube and the flow cell show that the 10 µL volume flushes were only marginally effective in the inlet tube. Small particles require a higher flow to be lifted off from the surface, because velocity drops to zero at the tube or flow-cell wall and a small particle does not extend far into the flow field. However, very small particles (≈ 1 µm) do not have time to sediment to the bottom of the inlet tube, which has a diameter that is 7× larger than the flow-cell thickness. As a result, sedimentation is of greatest concern for intermediate particle sizes. The small-volume flushes were insufficient to fully clear the particles that sedimented to the bottom of the flow cell, and the number concentration increased. The values reported for RM 8634 used only data obtained with the 20 µL pulses.

14

To further verify that mixing was uniform for all runs and to understand possible inhomogeneities in ETFE number concentration, FI measurements were taken for samples from the PETG vial (where the sample was stored before analysis) before the SFM run and from the SFM vial after the run was completed. This was done for both 2.5× and 5× concentrated samples. The results (data not shown) show that there is minimal difference in the PSD before or after SFM analysis. This means that the mixing was uniform and the particle concentration in the vial remained constant throughout the run.

The FI data, obtained from samples prepared for SFM runs, was adjusted for concentration and compared to the FI measurements of the actual RM 8634 vials, to show that the sample analyzed on the SFM is representative of the RM samples, even though it was at a higher concentration. The FI measurements were first adjusted for dilution and cell thickness. The adjusted concentrations were compared to one another (2.5× versus 5×), to give an indication of the FI linearity; no statistically significant differences were apparent. Additionally, the scaled FI measurements were compared to the RM 8634 FI measurements. When the ratio of those two data sets were compared, there was a small, statistically significant difference (Student's t-test, $p < 0.05$) for size ranges 2 µm to 3 µm and ≥ 15 µm. We multiplied all SFM number concentrations by a bias factor to account for this difference between the SFM vials and the actual RM 8634 vials and included the experimental standard deviation of the mean (ESDM) of this bias in the uncertainty budget.

3.3.3. Data Analysis

The SFM images were first cropped to remove edge particles and then analyzed by ImageJ to apply a binary threshold and then two dilations, a fill, and two erosions to reduce particle fragmentation. From the resulting binary image, ImageJ was used to count and characterize the size and morphology of the particles. A Python script analyzed the ImageJ output to remove stuck particles. In Excel, a measurement frame was applied and particles with a center of mass outside a defined frame were discarded. Unlike the FI analysis, the region outside the measurement frame was 40 pixels wide around the full periphery of the image (whereas it was 30 pixels from the left and right on the FI images).

3.3.4. Uncertainty of Stop-Flow Microscope PSD Measurements

For the SFM, the most significant uncertainty components are sedimentation and flushing of particles, for the ≥ 2 µm to ≥ 10 µm size limits, and repeatability related to limited particle number for size limits of ≥ 7 µm and larger. The uncertainty of the diameter corrections is significant for all size limits, and dominant for size limits of ≥ 15 µm and higher.

Initial inspection of the SFM results showed a pronounced sensitivity on flush volume, such that the 10 µL flush runs were considered unreliable and the 20 µL flush runs could be trusted. We also measured the ETFE sample before and after most SFM runs using FI. This large body of FI data on the concentrated ETFE samples was scaled to the concentration of the RM vial samples by dividing measured number concentration by the gravimetrically determined dilution factors. The number concentration ratio for the RM vials to the SFM samples was measured by FI to determine the equivalence of the dilution-factor corrected SFM samples with the RM vials. A small, but statistically significant, difference was observed, and a correction factor for the bias of the SFM samples relative to the RM vial

15

samples was included. The inclusion of FI data for ETFE drawn from the stock-solution vial before an SFM run and for ETFE drawn out of the stirred vial on the SFM after a run ensured that the correction factor accounted for sample evaporation as well as any other differences in ETFE number concentration between the samples.

3.4. **Palmer Chamber**

Optical microscopy measurements using the Palmer chamber (PC) provide a cross-check on the SFM measurements and have no sample settling or flushing issues. The PC (Hausser No. 3850, Horsham, PA, USA) is a glass microscope slide with a coin-shaped depression approximately 400 µm deep and a cover slip. The well-defined depression assures that the sample volume is highly repeatable. Like the SFM measurements, the number of particles measured is relatively low, so we measured the same 5× concentrated sample as used for the SFM.

3.4.1. **Instrument Set-Up & Sample Acquisition**

The PC was cleaned by scrubbing with semiconductor-grade knit polyester swabs and detergent solution. The 5× concentrated ETFE sample was handled as described below in Section 6.2. While the ETFE foam was dissipating, a moistened folded paper towel was placed beneath an inverted 100 mm crystallization dish. Evaporation of water from the towel increased the humidity under the dish.

The PC was filled from above with 135 µL of ETFE sample, drop by drop, with the pipette tip moving laterally so the drops were deposited uniformly across the chamber area and the cover slip placed on. The cell was tilted to remove any small bubbles out of the fill ports. The filled sample was placed under the upside-down crystallization dish with the moistened towel, and the ETFE particles allowed to settle for 30 min. The humid environment inhibited evaporation of the PC sample. The same procedure as above was used for blanks, where the ETFE sample is replaced by diluent.

The filled PC was imaged under an upright optical microscope (model DMR, Leica Microsystems, Inc., Buffalo Grove, IL) with a 10×/0.30 NA objective, a 455 nm wavelength LED light source (identical to the SFM light source) set for Köhler illumination. Images were acquired with an Infinity 2-2M camera. The pixel size of the images was determined with a calibrated stage micrometer, by the same procedure as was used with the SFM, described in Section 3.3.1 above. Image acquisition began ≈ 1 mm from the chamber edge at one side of the slide. The focus was adjusted by first finding the focal knob position where the smallest particles had the lowest visible contrast (the wash-out point). Then the stage was moved vertically by 6 µm, in the direction that makes particles darker in their interior, identically to the SFM focus procedure. The PC surface was imaged in a raster scan, with images 2 mm apart in *x* and *y* directions and refocused every other image; typical runs had 25 to 35 images. This scan was performed quickly to minimize sample evaporation. Data acquisition ceased when the bubble from the side ports grew to more than 20 % of the chamber area or when multiple, small, out-of-focus particles appeared in the field of view.

The cell thickness is nominally 400 µm. A correction factor was obtained by analyzing multiple runs of polystyrene latex (PSL) microsphere suspensions that had been measured for absolute number concentration on the LO instrument and determining the ratio of number

concentration from the LO instrument versus the PC. That ratio is equal to the ratio of (400 µm)/(actual thickness). Background concentration measurement of the diluent was found to be negligible.

3.4.2. Data Analysis

Images were analyzed in ImageJ as a stack. Any images with visible out-of-focus particles, air bubbles, or cell edges were first discarded. The median of the stack at each pixel location was used as a background image, and the stack divided by the background image and rescaled. The remaining ImageJ analysis steps were the same as for the SFM, except that the binary threshold was set at 94.5 % of the median intensity rather than 96 %, because of the higher noise for the SFM camera.

The data output from ImageJ were copied into an Excel template that applied corrections for cell thickness, concentration factor, and deviation of the 94.5 % threshold from the 96 % threshold used for diameter calibration. Some data sets showed a large scatter in results. Inspection of the images showed that sample evaporation could lead to incursion of extraneous particles and air bubbles. We discarded any runs that had a large difference (more than 3 SD) of particle numbers from the front half to the back half of the image set, or that had at least two of the following flaws: clear instances of particle transport, multiple images with non-settled particles, or apparent extraneous particles (other than ETFE).

3.4.3. Uncertainty of Palmer Chamber PSD Measurements

For the PC measurements, the most significant uncertainty component is poor reproducibility for size limits of ≥ 7 µm and above, which is linked to inhomogeneous particle deposition. In addition, the uncertainty of the diameter corrections is significant for size bins up to ≥ 15 µm. The variability of the PC data was larger than anticipated from Poisson statistics alone. Two runs in particular had minimal signs of extraneous, foreign particles, but the number of large particles was quite high, and the particles were not evenly distributed over the acquired image frames. It is likely that the larger ETFE particles are either not being deposited uniformly or are shifting during the sample preparation or slide transfer process.

Because the PC measurements were performed on ETFE samples that were 5× more concentrated than the RM vial samples, and because the PC cell thickness is nominally 4× thicker than the FI cells that we used, the PC images have a substantially higher number of particles per unit area (≈20× higher than the FI images). We assessed possible coincidence errors by analyzing the PC images as single images, and also by artificially merging sets of two images into a single composite image. Results of this analysis show that the coincidence error is quite small: 0.4 % of the number concentration or less, for all size bins.

The diameter uncertainty and the uncertainty for scaling the number concentration for the 5× sample to the RM vial concentration are the same as for the SFM. To account for the shift in particle diameter that occurred on use of a smaller threshold value than the calibration runs, four runs of SFM images were analyzed at the calibration threshold value (96 % of the median intensity) and at the value used for the PC runs (94.5 % of median intensity). A correction factor for particle counts was obtained by taking the ratio of number concentrations for these two sets of analyses. The relative ESDM of this correction factor

was taken as the standard uncertainty. (The analysis was performed using SFM data because the image-intensity noise of the PC images is too high for analysis at the 96 % threshold.)

4. Morphology Measurements of RM 8634

4.1. Overview

Morphology-related terminology in the field of particle analysis is not standardized. We have chosen to follow to a large extent the conventions in ISO 9276-6 [12] with some minor changes in notation to avoid multiple levels of subscripts. The morphological parameters chosen for reported reference values do not include any that depend on particle perimeter, since the perimeter is especially sensitive to pixel size and image resolution.

Particle morphology was measured by three instruments: 1) the same SFM as described above, 2) the same PC measurements as described above, and 3) a scanning electron microscope (SEM), for which particles were captured on porous alumina (Anodisc) filters. For the SFM and PC measurements, the same optical images used for determination of the PSD were used to generate distributions of morphological parameters. ImageJ was used to evaluate the morphological parameters for the particles identified in the binary images. Artificial particle images were used to verify the accuracy of the ImageJ calculations.

4.2. Stop-Flow and Palmer-Chamber Morphology Measurements

The morphological parameters reported for this RM, as measured from the binary images, can be expressed in terms of basic length measurements of the binary image, as follows. The ellipse ratio equals the ratio of minor and major axes ($L_{\min}$ and $L_{\max}$) of the ellipse with the same area and ratio of second moments as the measured particle:

$$f_{\mathrm{ell}} = \frac{L_{\min}}{L_{\mathrm{maj}}} \quad . \tag{2}$$

The aspect ratio equals the ratio of minimum and maximum Feret diameters ($F_{\min}$ and $F_{\max}$):

$$f_{\mathrm{asp}} = \frac{F_{\min}}{F_{\max}} \quad . \tag{3}$$

The compactness equals the ratio of equivalent circular diameter to the maximum Feret diameter:

$$f_{\mathrm{comp}} = \frac{d_m}{F_{\max}} \quad . \tag{4}$$

Figure 6 displays these definitions graphically:
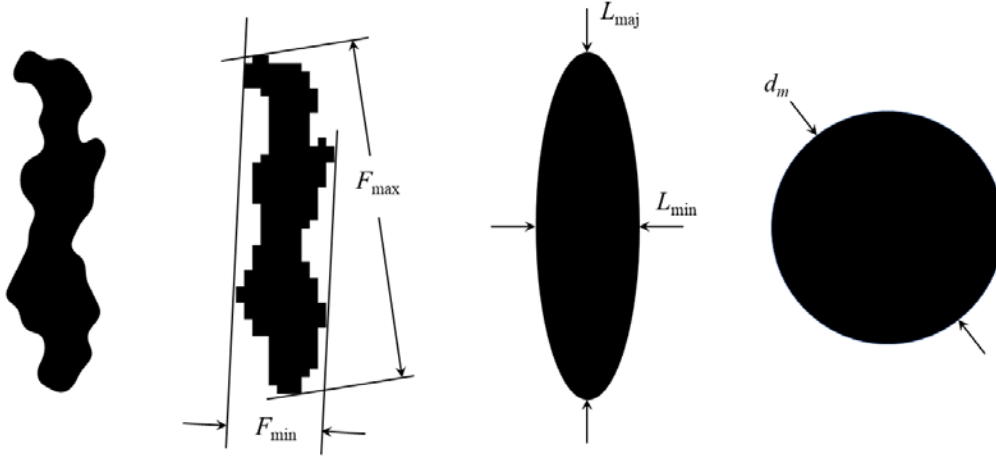
Figure 6. Characteristic dimensions of a binary particle image.

The bias correction for the morphological parameters assumes that optical diffraction and out-of-focus effects expand the periphery of the binary image by a distance δ, as shown in Figure 7.
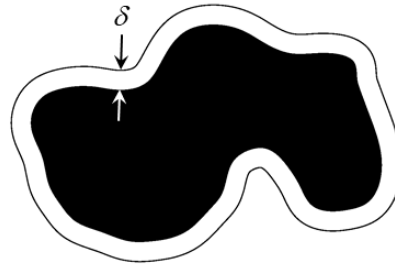
Figure 7. Original binary particle boundary (outline) and corrected particle (solid).

The corrected morphological parameters are then:

$$f'_{ell} = \frac{L_{min} - 2\delta}{L_{maj} - 2\delta} \tag{5}$$

$$f'_{asp} = \frac{F_{min} - 2\delta}{F_{max} - 2\delta} \tag{6}$$

$$f'_{comp} = \frac{d}{F_{max} - 2\delta} \quad . \tag{7}$$

To implement these corrections, the quantity δ is related to the diameter difference Δd between measured (d_m) and actual (d) particle diameters. Because δ adds area along the whole particle perimeter, the proportionality between δ and Δd depends on an effective value of the circularity f'_{cir} (where circularity, f_{cir}, is defined by $f_{cir} = P/\pi d$ with P the particle perimeter; derivation of the effective circularity not shown):

$$\delta = \frac{\Delta d}{2} f'_{cir} \tag{8}$$

$$f'_{cir} = \frac{(d_m + d)}{(d_m / f_{cir,m} + d / f_{cir,a})} \quad . \tag{9}$$

19

The circularity of the measured particle is obtained from ImageJ output (although the ImageJ definition is the square of the ISO definition used here) and we approximated the circularity of the actual particle using a fit of the SEM data.

4.2.1. Uncertainty of SFM and PC Morphology Measurements

The results for the morphological parameters show very little variation as a function of particle equivalent circular diameter for the mean of the three methods (SEM, SFM, and PC). The reported parameters are also dimensionless ratios of reported lengths. As a result, errors in the equivalent circular diameter have a negligible effect on the uncertainty of the morphological parameters.

The corrected morphology parameters depend on δ, so an error in δ will cause an error in the morphology parameters. The uncertainties were obtained by first using the relation $\delta = f'_{cir} \Delta d/2$ to express Eqs. 5 to 7 in terms of Δd instead of δ, and then using the Law of Propagation of Error to find the uncertainty. The uncertainty component related to Δd is the dominant component in the uncertainty budget.

The ellipse-ratio uncertainty, $u(f_{ell})$, was obtained by assuming that the ellipse ratio was proportional to the aspect ratio for different particles ($f_{ell} = \alpha f_{asp}$), and then algebraically solving for $u(f_{ell})$ in terms of $u(f_{asp})$. The value of α varies with size and measurement method but is within the range 0.9 to 1.1 (data not shown). Using mean values for f_{asp} and f_{comp}, we obtain

$$u\left(f_{ell}\right) \approx 1.25\, u\left(f_{asp}\right) \quad . \tag{10}$$

The ellipse ratio correction in Eq. 5 reduces the minor and major axes of the Legendre ellipse by 2δ. However, the Legendre axes are not the same as actual image lengths. An alternate approach is to assume that the ellipse ratio scales in the same manner as the aspect ratio:

$$f'_{ell} = f_{ell} \cdot \frac{f'_{asp}}{f_{asp}} \quad . \tag{11}$$

The deviation between Eq. 5 and the scaling approximation of Eq. 11 is added as a component to the uncertainty budget. See Appendix C for tabulated uncertainty values.

4.3. Scanning Electron Microscopy

For the SEM measurements, concentrated ETFE solution was vacuum filtered to deposit the particles onto anodized alumina filters with a nominal 0.2 µm pore size (Whatman Anodisc 25 mm diameter with support ring, GE Healthcare Life Sciences, Marlborough, MA) that had been previously cleaned and metallized with 30 nm of Au/Pd. After particle deposition, an electrically conductive top coat was deposited. The SEM image data was collected on a TESCAN MIRA-3 Schottky field-emission SEM with an Everhart-Thornley secondary electron (SE) detector and an yttrium-aluminum-garnet scintillator back-scattered electron (BSE) detector. The automated [13,14] SEM collected a set of both SE and BSE images at 15 keV beam energy, a working distance of 17 mm and approximately 1 nA probe current, with a 62.5 µm field of view. To calibrate the pixel scale, a series of images were collected from a Geller MRS-4XY (s/m R23-104) magnification standard, which itself was calibrated using the NIST Line Scale Interferometer [1]. Images obtained with the SE detector had better particle contrast than images obtained with the BSE detector. Only a small fraction of

the filter area was sampled (approximately 1000 images). Additional runs were also conducted to measure an Anodisc after filtering diluent with no ETFE ('blank').

4.3.1. SEM Data Analysis

The pores of the Anodisc filters make effective electron traps and appear very dark when not covered by an ETFE particle. If the detected pores are connected over a short length scale, the regions that have neither pores nor connecting lines are identified as particles.

SEM images (see Figure 8A) were analyzed by thresholding the images in ImageJ, choosing a threshold value such that the pores were identified as much as possible while limiting the number of thresholded pores or crevices in the interior of ETFE particles (Figure 8B). Following conversion to a binary image, a custom Fortran program drew lines between nearby pores. Particles appeared as those regions with no (or minimal) lines (Figure 8C). Further processing in ImageJ by a single cycle of erosion, dilation, and filling gave clearer images. Inspection of the resulting original and binary images showed a substantial number of Anodisc defects that were identified as particles. The binary images were edited by hand to remove traces of these defects, using the original images as guides (Figure 8D). Particle images were also edited to erase single, thin lines bisecting particle images, or to otherwise join split particle images to match the original images. If the particle connectedness was hard to discern, the particle was erased from the image. Particle morphology parameters were determined using the Analyze Particles feature in ImageJ, and the results were tabulated.
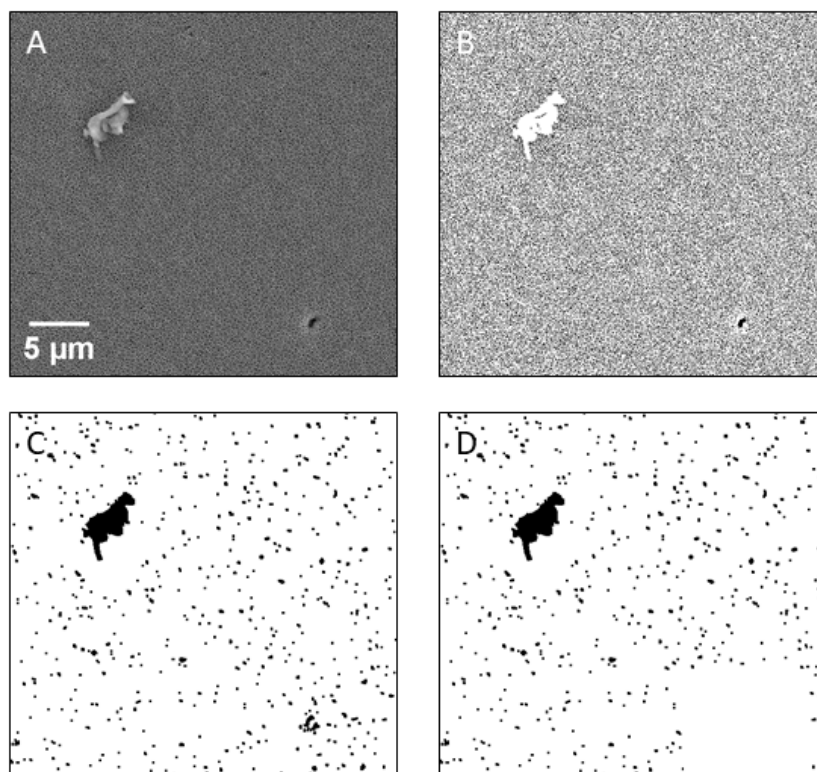
Figure 8. (A) Digital SEM image, (B) binary image after threshold application, (C) output of SEM_Pore.f90 connecting black regions in (B) and then inverting black and white, and (D) result of manual editing to remove Anodisc defects.

21

4.3.2. Uncertainty of SEM Morphology Measurements

Statistical variation of the morphological parameters was assessed by binning the particles by equivalent circular diameter and then finding the ESDM for each bin of each parameter. This variation was only significant for particles with $d > 2$ µm because of the low numbers of large ETFE particles in the SEM data sets. Depending on the alignment of a particle edge with the Anodisc pores, the particle outline formed from lines connecting the pores can either overestimate or underestimate the extent of the particle. To assess the magnitude of this effect, we hand drew boundaries of 30 magnified SEM particle images, analyzed the filled shapes, and compared these results to the automated-analysis results. The difference between hand-drawn and machine generated morphological parameters was taken as one standard uncertainty. The effect of background particles on the morphological parameters was determined by the same method used for the PC and SFM date, in which particle data from a background run was artificially added to the results of a particle counting run. See Appendix C for tabulated uncertainty values.

5. Results

5.1. Combined PSD Results

Figure 9 shows the combined PSD data sets. Despite our significant efforts at diameter calibration, FI results after correction of diameter biases agreed with other methods only for $d > 7$ µm. For reasons described earlier (Section 3.2.3), we discarded FI data below 7 µm.
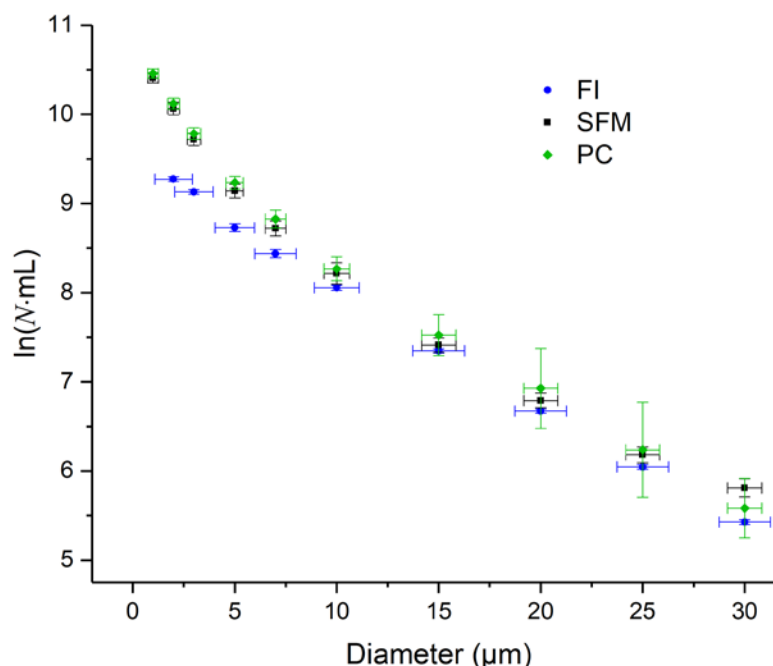
Figure 9. Measurements of the PSD by three methods. Uncertainty bars for individual data points are standard uncertainties.

22
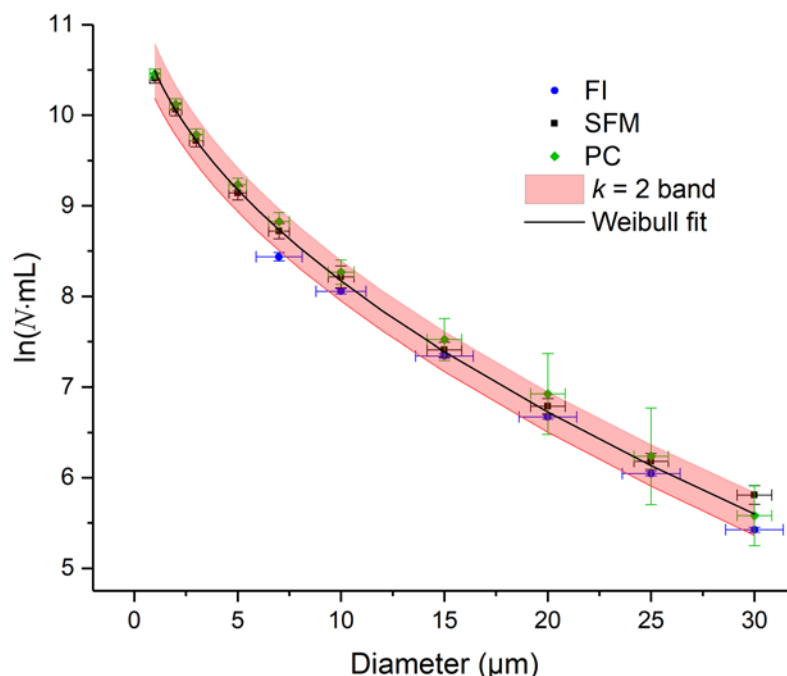
Figure 10. Data and best fit for the PSD. Uncertainty bars for individual data points are standard uncertainties.

Equations for the propagation of uncertainty presume that the measurand is approximately a linear function of the input parameters, within the range of the uncertainties. The values of $N(d)$ violate this assumption since $N(d)$ rises very rapidly with decreasing diameter. To address this issue, we transform the PSD data and use $\ln(N)$ instead of N. On doing so, the plot is smoothly varying and linear at small and large diameters. A trial fit modeling $\ln(N)$ as a Weibull function,

$$\ln\left[N\left(d\right)\right]=\ln\left(b_0\right)-\left(b_1 d\right)^{b_2} \quad , \tag{12}$$

showed good agreement with the data, where b_0, b_1, b_2 are constants. The Weibull function has the advantage that it has an explicit inverse function, which greatly simplifies application of RM 8634 by the user.

The diameter uncertainty is strongly correlated between the PC and SFM, but only weakly correlated between FI and both the SFM and PC data sets. A reasonable approach is to assume complete correlation between PC and SFM data sets, and no correlation between FI and the other sets. Some additional degree of correlation of results for different diameters is expected because $N(d)$ includes the counts for N at diameter limits higher than d.

For each diameter, weighted means were obtained by combining the PC, SFM, and FI data sets, with diameter uncertainties propagated to an equivalent number concentration uncertainty and accounting for the correlations mentioned above. As shown by the solid black line in Figure 10, a Weibull function was fit to this data by the method of weighted least squares. The results for number concentration as a function of equivalent diameter are given by:

$$N(d) = b_0 \exp\left[-\left(b_1 d\right)^{b_2}\right]$$ (13

with

$$b_0 = 96\,727.7 \text{ mL}^{-1}$$
$$b_1 = 0.983\,21 \text{ μm}^{-1}$$ (14
$$b_2 = 0.523\,46$$

The inverse of the $N(d)$ function is:

$$d = \left(\frac{1}{b_1}\right)\left[\ln\left(\frac{b_0}{N}\right)\right]^{1/b_2} \quad .$$ (15

Table 1 gives the values of $\ln[N(d)]$ and $N(d)$ at discrete values of d, along with the expanded uncertainties of these values. The expanded uncertainty of N is calculated using the approximation $U(N) \approx N \cdot U(\ln N)$.

Table 1. Reference values for the complementary cumulative distribution $N(d)$ in RM 8634.

Diameter, d (μm)	$\ln(N \cdot \text{mL})^{(a)}$	$N^{(a)(b)}$ (mL^{-1})
1	10.49 ± 0.31	35 900 ± 11 223
2	10.05 ± 0.27	23 270 ± 6 322
3	9.72 ± 0.25	16 615 ± 4 209
5	9.18 ± 0.25	9 682 ± 2 381
7	8.73 ± 0.22	6 215 ± 1 380
10	8.17 ± 0.23	3 538 ± 823
15	7.39 ± 0.23	1 618 ± 373
20	6.72 ± 0.22	832 ± 181
25	6.14 ± 0.22	462 ± 102
30	5.60 ± 0.24	270 ± 65

[a]Values are expressed as $x \pm U(x)$, where x is the reference value and $U(x)$ is the expanded uncertainty of the reference value with a coverage factor of 2. To propagate this uncertainty, treat the reference value as a normally distributed random variable with mean x and standard deviation $U(x)/2$.
[b]The propagation of uncertainty is based on the linear approximation $U(N) \approx N \cdot U(\ln N)$.

5.2. Combined Morphology Results

Particle morphology was determined from two SEM runs, eight SFM runs, and four PC runs. We analyzed optical and SEM image data for three morphological parameters: aspect ratio, ellipse ratio, and compactness. Inspection of the variation of morphological parameters versus diameter, as shown in Figure 11, demonstrates that there is very little dependence on diameter. As a result, calibration of any of the methods for absolute diameter is not critical. For all three parameters, the three methods give results generally consistent within combined uncertainties. For both PC and SFM data, the bias corrections are larger than the standard uncertainties for the lower size bins. These corrections are important corrections to achieve results consistent with the SEM results.

The morphology analysis is similar to that of the PSD data, except there is no fitting to a function or propagation of diameter uncertainty. The procedure for each of the three f morphology parameters is:

1. For each size bin, combine the PC and SFM values using an unweighted mean. The standard uncertainty of this value is taken as the mean of the PC and SFM uncertainties.
2. Obtain the reference value by taking the weighted mean of the f values for the SEM and combined PC/SFM data sets, over all size bins.
3. Calculate the uncertainty of the reference value by first finding the mean for all size bins of the SEM and PC/SFM data sets, and then calculate the weighted uncertainty of these two values.

The ETFE particles are highly variable in morphology, and the standard deviation SD of the measured values (shown in Table 2) characterizes the variability of the ETFE particle population. The agreement between methods is reasonable, but there is a significant problem in the data set. Even within a single method, SD varies from size bin to size bin more than would be expected on statistical grounds. SD is a material property, and not just a component of the measurement uncertainty. The SD values of the three morphological parameters are plotted in Figure 12. The uncertainty bars in Figure 12 represent the ESDM for the individual PC and SFM runs (or the predicted ESDM based on counting statistics for the SEM measurements). The SFM and PC data are not consistent within the experimentally observed repeatability, and the SFM data has larger variations with diameter than expected from counting statistics alone. Each measurement method may have unknown sources of variability unrelated to counting statistics that cause bias in the observed standard deviation. We are unaware of any errors that could cause such behavior. Consequently, taking a weighted mean is not appropriate. Instead, the simple mean of all data is taken as the best measure of SD, with standard uncertainty of this mean value equal to the standard deviation of the SD values in the size region where all three methods are used divided by the square root of three (i.e., assume the effective degrees of freedom equals the number of methods used).
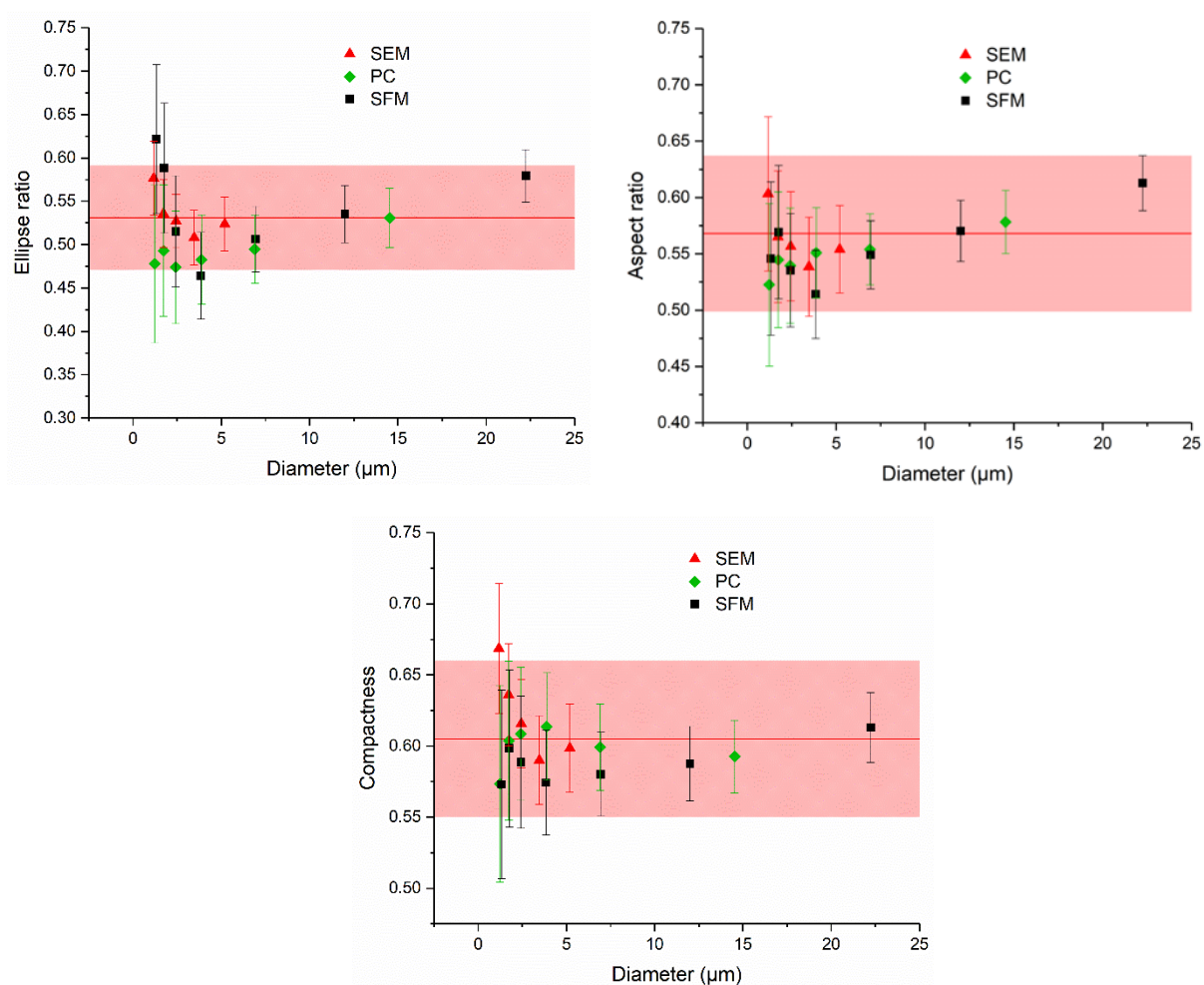
Figure 11. Morphological parameters as a function of diameter. Uncertainty bars give the standard uncertainty of individual points, and the band is a $k = 2$ confidence interval.
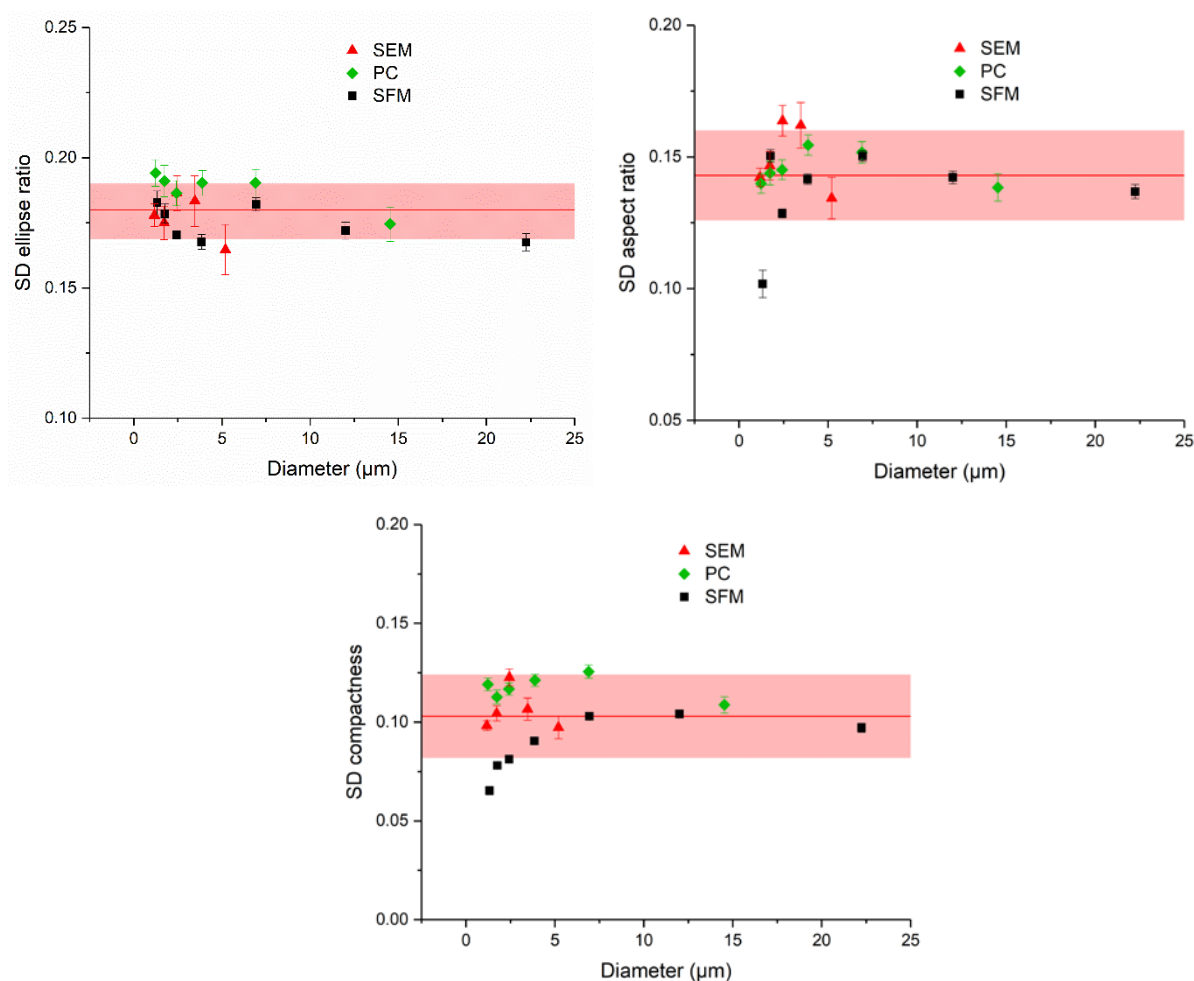
Figure 12. Standard deviation *SD* of the morphological parameters as a function of diameter. Uncertainty bars give the standard uncertainty of individual points expected from Poisson statistics. The band is a *k* = 2 confidence interval.

Table 2. Reference values for morphological parameters in RM 8634

Parameter	Mean Value[a]	*SD*[a]
f_{ell}	0.531 ± 0.060	0.180 ± 0.010
f_{asp}	0.568 ± 0.069	0.143 ± 0.017
f_{comp}	0.605 ± 0.055	0.103 ± 0.021

[a] Values are expressed as $x \pm U(x)$, where x is the reference value and $U(x)$ is the expanded uncertainty of the reference value with a coverage factor of 2. To propagate this uncertainty, treat the reference value as a normally distributed random variable with mean x and standard deviation $U(x)/2$.

27

6. General Handling and Storage Procedure for RM 8634

6.1. Maintenance and Storage of RM 8634
The ETFE particles are highly chemically inert as supplied. The ETFE RM vial should be stored in the refrigerator at (2 to 8) °C up to three years with minimal change (< 10 % change in the PSD and morphology) or at room temperature for up to one month.

6.2. Resuspension
ETFE particles will settle to the bottom of the vial. At the beginning of each day of analysis, the ETFE particles must be resuspended. First, the vial should be allowed to come to room temperature. Then, an effective way of resuspending particles is to ensure that the vial is firmly sealed, then hold the vial horizontally in your hand, with your forearm vertical, and shake back and forth **vigorously** for 20 s (at about 2 back-and-forth shakes per second). Because of the surfactant in the formulation, this procedure will generate a significant amount of foam. Allow the vial to sit for 60 min to 90 min for the foam to dissipate. Slowly tipping and rotating the vials 10 times every 30 min can increase the rate of foam dissipation. Do **not** sonicate to degas the solution. We have not found it necessary to do any additional degassing.

If the sample has been stored for longer than 1 week, it is most effective to shake the sample for 20 s the day before analysis, allow it to sit overnight at room temperature, and then perform the procedure (as described above) on the day of analysis.

Between measurements, particles will still be in suspension, but there will be some sedimentation. First ensure that the vial is firmly sealed, then hold the vial horizontally in front of you. Tip the vial gently from side to side 10 times, while slowly rotating the vial with each tip. With each tip, the air bubble in the vial should go from one end of the vial to the other. This gentle tipping method should be conducted before transferring material or taking a measurement whenever the vial has sat for more than 10 s. After performing the long-term-storage resuspension (vigorous shaking, as described above), we have confirmed that the gentle tipping method suffices to resuspend particles over the course of 5 h at a minimum.

After 2/3 of the sample has been used, it becomes harder to obtain a homogeneous sample from the vial, because of the settling of the larger particles. In addition, repeated opening and closing of the vial can lead to higher chances of contamination. Due to these factors, the last 10 % of the vial contents should not be used.

6.3. Vial Choice and Repackaging
The vial and cap are fabricated from PFA. Care must be taken to tighten the caps firmly to eliminate leakage. At the same time, excessive torque can lead to production of additional large particles. Friction on the threads of the PFA vials occasionally generates particles. These particles are not an appreciable fraction of the ETFE particles, except at large (>50 µm diameter) sizes. For this reason, the counts at large particle sizes may have poor repeatability. It is also important to avoid scratching the inside of the cap or vial.

When multiple draws will be taken from a RM 8634 vial within a month, thread debris can be minimized by first resuspending the ETFE particles and then transferring the particle

28

solution to precleaned polyethylene terephthalate (PETG) vials. PETG vials have minimal thread debris. Long-term storage in PETG is not recommended because extraneous small particles (< 2 µm typically) may appear after one month.

6.4. Allowed Treatment

The RM 8634 particle solution may be transferred by pipette, provided the suspension is mixed just prior to transfer (see Section 6.2). Pipette tips should either be confirmed to contribute low particle loads (e.g., pipette tips with built-in barriers) or be thoroughly rinsed before use.

The RM 8634 particle solution may be diluted with water/glycerol mixtures to reduce the optical contrast of the ETFE particles, as described in Section 9, or with water. The RM 8634 solution should not be diluted by more than a factor of one part of RM 8634 to three parts of diluent (by volume), to ensure that there is sufficient surfactant in the final solution to prevent ETFE agglomeration.

6.5. Detrimental Treatment

The following sample handling methods should be avoided:
- Do not centrifuge: centrifuging causes particles to entangle and inhibits resuspension.
- Do not sonicate: sonicating has been shown to damage the PFA vial.
- Do not vortex: vortexing is inefficient at resuspending particles, and the circular path of the particles rubbing against the interior vial surface generates additional particles.
- Do not place for long periods on a vial tumbler: with extended rotation, the particle motion against the side of the vials breaks down the large particles.
- Do not freeze.

7. Correcting Reported Diameters Using RM 8634

The RM 8634 material can be used to correct the reported diameter of particle counting instruments. Prior to determination of this correction, the instrument should be verified for accurate particle diameter and number concentration measurements following manufacturer recommendations. Instrument settings used for these verification steps may differ from the settings used for ETFE and test samples. The hardware and software settings for subsequent tests of user samples should be the same as used for the ETFE.

For polydisperse distributions of particles, an error in reported diameter can cause an error in reported number concentration. For example, if 10 % of the particles above 10 µm are incorrectly sized as under 10 µm, the reported number concentration of particles above 10 µm will be too low by 10 %.

This section describes a method to determine what diameter reported by the instrument corresponds to the ETFE-diameter reference values. The instrument response, and the nature of the correction table, will depend on a variety of factors:
- the hardware configuration of the instrument (e.g., magnification for flow imaging instruments, light obscuration sensor head model);

- the software configuration (e.g., threshold settings for FI instruments); and
- whether the optical contrast of the ETFE has been adjusted by mixing with water/glycerol solutions.

When the suspension of ETFE particles is measured in a user's particle counting instrument, the reported particle concentrations can be tabulated as the reported number concentration of particles N_{rep} greater than a reported diameter, d_{rep}. Table 3 gives hypothetical data obtained with a user's particle counting instrument, for diameter and number concentration of the RM 8634. The subscript k denotes the kth line in the table.

Table 3. Hypothetical values for N_{rep} and d_{rep} obtained from a user instrument for RM 8634. The index k refers to the row number in the table.

k	$d_{rep,k}$ (μm)	$N_{rep,k}$ (1/mL)
1	1	27 991
2	2	17 657
3	5	6 704
4	10	2 016
5	15	700
6	20	233
7	25	52

We seek the ETFE diameter (d, defined in Equations 14 and 15) that corresponds to the reported instrument diameter (d_{rep}). The basic method is to find the RM reference-value diameter d where the number concentration value from the Report of Investigation is equal to the reported number concentration from the instrument, $N_{RM} = N_{rep}$. In effect, we are assuming that the user instrument counts each particle but assigns an incorrect size to the particle. (This assumption is supported by the success of diameter scaling at reconciling differences between different particle count instruments [2].)

A simple method to determine these corresponding values is to use an inverse function that expresses the RM 8634 diameter as a function of number concentration. Equations 14 and 15 give the inverse equation for RM diameter as a function of number concentration.

To correct the diameter readings of an instrument, the user first takes one pair of $d_{rep,k}$ and the corresponding $N_{rep,k}$. The value of $N_{rep,k}$ is inserted into Eq. 15 in place of N_{RM}, and a value of d_k obtained:

$$d_k = \left(\frac{1}{b_1}\right)\left[\ln\left(\frac{b_0}{N_{rep,k}}\right)\right]^{1/b_2} \quad . \tag{16}$$

This process is repeated for all sets of ($d_{rep,k}$, $N_{rep,k}$). The result is a set of actual diameters that correspond to the set of reported values.

See Figure 13 for a schematic of this process.

30
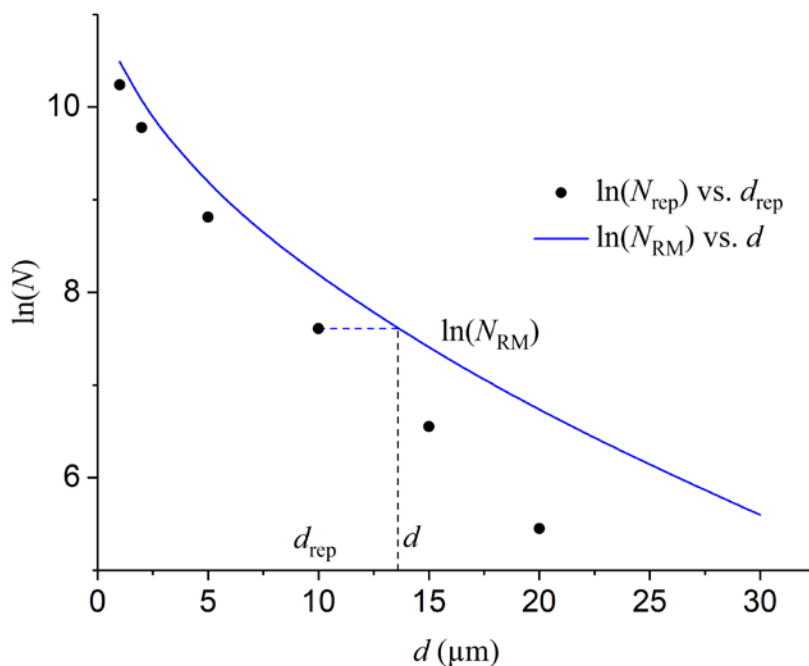
Figure 13. Finding the value of d corresponding to d_{rep} by setting $N_{RM} = N_{rep}$, and using an inverse equation.

As an example, suppose that we wish to find the ETFE-diameter reference value that corresponds to an instrument reported diameter of 10 µm. Referring to Table 3, the measured number concentration for $d \geq 10$ µm is 2 016 mL^{-1}. The value of d is obtained by using this value as well as constants from Equation 14 and putting them into Equation 15, to obtain the following:

$$d_4 = \left(\frac{1}{0.983\,2} \right) \left[\ln \left(\frac{96728 \text{ mL}^{-1}}{2016 \text{ mL}^{-1}} \right) \right]^{1/0.5235} \mu m = 13.5 \,\mu m \quad . \tag{17}$$

The result $d_4 = 13.5$ µm from Eq. 17 is the diameter that corresponds to the reported diameter $d_{rep,4} = 10$ µm. In other words, this instrument reports 13.5 µm ETFE particles as having a diameter of 10 µm. Application of Eq. 17 to the data in Table 3 generates the following correspondence table for d_{rep} and d_k:

31

Table 4. Corresponding reported and reference diameters, for the hypothetical data from Table 3.

k	d_k (μm)	$d_{\text{rep},k}$ (μm)
1	1.53	1
2	2.81	2
3	6.63	5
4	13.50	10
5	21.41	15
6	31.46	20
7		25

Once a correspondence table has been created for a particular instrument and instrument setting, that table can be used to correct the diameter readings of the instrument. Note that this correction is valid for protein particles that are similar in optical properties to the ETFE sample but will not be valid for protein samples containing a large number of particles with very different optical properties (e.g., small rubber, metal particles, or silicone oil droplets).

8. Using RM 8634 to Determine the PSD of an ETFE Working Standard

For routine testing of instruments, the cost of RM 8634 may be prohibitive. In this case, RM 8634 may be used to determine the PSD of a working standard comprising a suspension of ETFE particles produced in the same manner as RM 8634. Working standards may be fabricated by the user or obtained from commercial sources.

The first step is to generate a table (for example, Table 4 above) giving the correspondence between d_{rep} and d for a particular FI instrument, using the procedures in Section 7. Next, the working standard should be measured on the same instrument, with the same protocol as RM 8634, to obtain the particle number concentration of the working standard, N_{WS}, for the same set of reported diameters used for the first step. Once the pairs (d_{rep}, N_{WS}) are found, the correspondence table determined in Section 7 is used to find the values of d that match d_{rep}, giving a set of data pairs (d, N_{WS}) that gives the number concentration of the working standard versus a corrected diameter.

Because d is obtained by the inverse equation instead of the initial instrument settings, the data pairs will generally be at values of d that do not correspond to even values in micrometers. To generate a table of (d, N_{WS}) at even values, there are two options.

Option A. Using a non-linear fitting routine, fit an equation of the form

$$\ln N_{\text{WS}} = \ln c_0 - c_1 d^{c_2} \quad . \tag{18}$$

The resulting values of c_0, c_1, and c_2 can be used to generate values of $N_{\text{WS}}(d)$ by the equation

$$N_{\text{WS}} = c_0 \exp\left(-c_1 d^{c_2}\right) \quad . \tag{19}$$

32

Option B. The N_{WS} values for d values intermediate to measured points may be obtained by interpolation. Because N for the RM 8634 particle suspension rises rapidly with decreasing diameter, the most accurate way to perform this interpolation uses the logarithm of the number concentration. See Figure 14 for a schematic of this process.
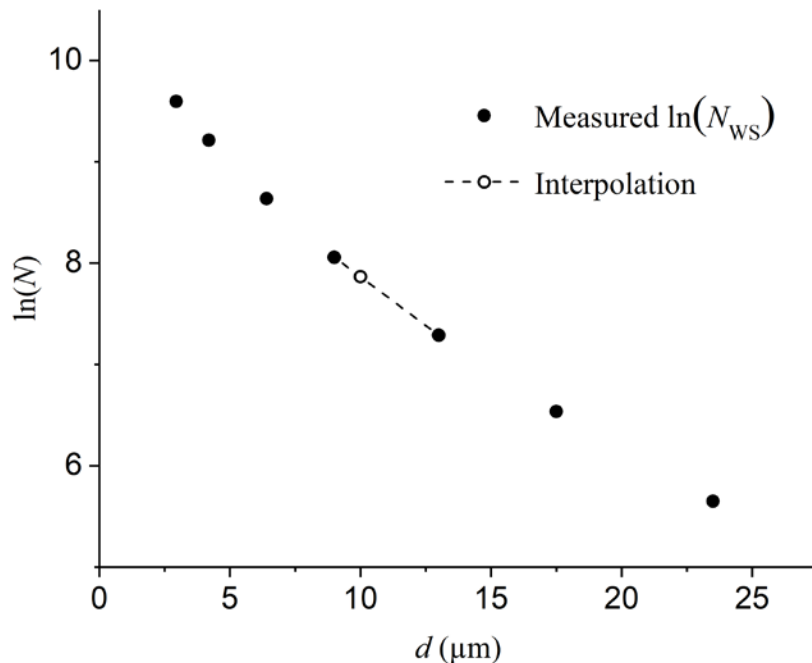
Figure 14. Logarithm of the working standard number concentration, ln N_{WS}, and interpolation to desired values of diameter d.

The equations to find the interpolated reported diameter that corresponds to a chosen diameter are:

$$\ln N_{WS} = \ln N_{WS,j} + s_j(d - d_j)$$
$$s_j = \frac{\ln N_{WS,j+1} - \ln N_{WS,j}}{d_{j+1} - d_j} \quad ,$$

(20

where d_j is the largest value that is still less than d, and d_{j+1} is the next value of d in the measured data set, and s_j is the slope of ln N_{WS} versus d. For example, suppose we wish to find the instrument reported diameter that corresponds to an actual ETFE diameter of 5 µm. Referring to Table 5, 5 µm is bracketed by the $j = 2$ and $j = 3$ entries. The interpolated value of N_{WS} is obtained from:

$$s_2 = \frac{8.843 - 9.376}{(6.48 - 4.21)\ \mathrm{µm}} = -0.2348\ \mathrm{µm}^{-1}$$

(21

$$\ln N_{WS} = 9.376 + (-0.2348\ \mathrm{µm}^{-1})(5.00 - 4.21)\mathrm{µm} = 9.191$$
$$N_{WS} = \exp(9.191)\ \mathrm{mL}^{-1} = 9\,805\ \mathrm{mL}^{-1}.$$

33

The result $N_{WS} = 9\,805$ mL^{-1} from Eq. 21 is the reported number concentration that corresponds to the calibrated diameter $d = 5$ µm. (The value in Table 5 differs slightly because the value of ln N_{WS} was not rounded in calculating N_{WS}.) In other words, this working standard has a number concentration of 9 805 mL^{-1} for ETFE particles of equivalent diameter ≥ 5 µm. Accurate application of Eq. 21 requires that the user data for N_{WS} be reported at the same bin width or smaller as for RM 8634.

Table 5. Hypothetical values for measured values of N_{WS} and ln $N_{WS,j}$ and interpolated values at even values of d. The index j refers to the row number in the table for the measured points, and s_j is the slope of ln($N_{WS,j}$) vs. d_j. Shaded rows give interpolated values.

j	d_j (µm)	$N_{WS,j}$ (mL^{-1})	ln($N_{WSj}\cdot$mL)	s_j (µm^{-1})	ln($N_{WS}\cdot$mL) (interpolated)	N_{WS} (mL^{-1},inter-polated)
1	2.95	16 865	9.733	−0.283 3		
	3.00				9.719	16 628
2	4.21	11 802	9.376	−0.234 8		
	5.00				9.191	9 804
3	6.48	6 926	8.843	−0.194 9		
4	9.23	4 052	8.307	−0.162 9		
	10.00				8.182	3 574
5	13.76	1 937	7.569	−0.140 3		
	15.00				7.395	1 628
6	17.48	1 149	7.047	−0.123 2		
	20.00				6.736	843
7	23.51	547	6.304			

9. Adjusting the Optical Contrast of RM 8634

The refractive index (n or RI) of ETFE is approximately 1.40. RM 8634 can be diluted into various concentrations of glycerol/water mixtures to reduce the refractive index difference between the ETFE particles and the matrix liquid, thereby mimicking the low optical contrast of especially translucent protein particles. As the refractive index difference is reduced, optical particle counters will give increasingly smaller sizes of the ETFE particles and the particle concentration will sharply decline. The procedure to dilute RM 8634 into glycerol/water mixtures is as follows:

1. Prepare the RM 8634 sample for analysis as described in Section 6.
2. Gravimetrically prepare ≈ 100 g of an 80 % mass fraction solution of glycerol-water.
3. This concentrated solution can be filtered using a 0.45 µm syringe filter with a PVDF membrane. Since this solution is viscous, filtering must be done slowly to ensure that the filter does not get damaged. The filter should be preconditioned with 5 mL water

followed by 5 mL of 80 % glycerol-water, both of which need to be discarded, before filtering the final solutions.

4. In clean PETG containers, prepare solutions containing different volumes of 80 % glycerol and RM 8634 to obtain a final mass of 15 g (See Table 6).

5. Glycerol concentrations should be kept above 20 % mass fraction and the RM 8634 should be diluted so that the number concentration of ≥ 1 µm particles is still above $2000\ \text{mL}^{-1}$ to obtain a sufficient particle number concentration. The table below serves as a typical example of the concentrations of the solutions used. The user should also prepare glycerol-water blanks at the same nominal glycerol concentration for each of these solutions to use for optimization of illumination in the FI. The last column shows the dilution factor for each solution, which is calculated as (Total sample mass) / (RM 8634 mass). Multiplying the reported FI number concentrations by this factor corrects for the dilution of RM 8634. This operation is performed on each solution to account for dilution effects so the effects due to the presence of glycerol, and corresponding RI differences, are more apparent.

6. After preparing the solutions and all controls, the solutions should be gently rolled and tilted in a way to mix the solutions without creating any bubbles. The Triton X-100 in RM 8634 can easily cause bubbles to form.

7. Determine the refractive index n_{gw} of the final solutions using a refractometer. Approximate n_{gw} values for a wavelength of 589 nm for the various solutions are shown below.

8. On the FI, run water blanks to ensure low particles. Before running samples containing glycerol-water, load 2 mL of DIUF to clean the tubing and flow cell. Let the flow cell run dry. Prime the instrument using the glycerol-water blank, at a flow rate slow enough to not generate voids or bubbles (e.g., 0.3 mL/min for typical FI instruments).

9. Gently rotate the ETFE-glycerol solution, at the same glycerol concentration as the solution in the flow cell, load the solution into the FI instrument, and start the run.

10. On completion of the run, purge the glycerol-water out of the flow cell at a rate of 0.3 mL/min for 30 s and then at default speed to get rid of any particles or the excess glycerol. Repeat these steps for all of the samples. It is important to prime with the corresponding glycerol blank before running the ETFE-glycerol solution at the same concentration. When loading the sample or removing the sample, first manually load the sample or water at a slow rate to not put too much pressure on the flow cell. Only when the majority of the glycerol has been removed from the flow cell, can the standard prime or flush options be used.

Table 6. Representative procedure for preparing various concentrations of glycerol-water solutions containing RM 8634 at different n_{gw}.

Solution	Mass of 80 % glycerol-water (g) (or diluent)	Mass of RM 8634 (g)	Final Mass (g)	Glycerol Concentration (% by mass)	Approximate n_{gw} (for those containing glycerol)	RM Dilution Factor $\dfrac{\text{total mass (g)}}{\text{RM 8634 mass (g)}}$
1	0	15	15	0	1.335	1.0
2	4	11	15	21	1.361	1.4
3	6	9	15	32	1.375	1.7
4	8.5	6.5	15	45	1.394	2.3
5	11.3	3.7	15	60	1.414	4.1

Typical results of this study conducted on the same FI instrument as used for RM 8634 are shown below in Figure 15, where the number concentration is plotted versus solution number (1 to 5 from the Table above). The number concentration of particles in four size bins (≥ 2 µm, ≥ 5 µm, ≥ 10 µm, and ≥ 20 µm) are monitored in these different solutions. The solid lines in Figure 15 show that the number concentration decreases up to $n_{gw} \approx 1.40$ (corresponding to solution 4) and then slightly increases after that. The slight increase in number concentration indicates that the particle refractive index is increasingly more negative than n_{gw}, and the optical contrast is increasing beyond the refractive index matching point. Reduced optical contrast will cause particles to be either undersized or fragmented. For typical applications of reducing the optical contrast of RM 8634, there is no need to prepare solutions with $n_{gw} > 1.40$. The dashed lines in Figure 15 show results for nearly identical samples that have been prepared as described in the Table above but the Triton X-100 solution replaced the 80 % glycerol solution; all of their RI are around 1.335. These solutions have been prepared to take into account dilution effects but not the RI effects due to the presence of glycerol.

The difference in the number concentrations for the 'without glycerol' compared to 'with glycerol' solutions are at a maximum for solution 4 (with $n_{gw} \approx 1.39$), where a 4 to 5 fold lower number concentration is observed for the glycerol containing solution (depending on the size bin).

Table 6 gives the dilution factors, which can be used to correct for the dilution of RM 8634 in this experiment. One can apply the procedures in Section 7 to find the reported instrument diameters corresponding to actual ETFE diameters for these solutions of RM 8634 in glycerol-water. The reported diameters will become increasingly smaller as the glycerol-water concentration is closer to the refractive index matching point.

Exact procedures for matching RM 8634 to a given population of protein particles have not been established and are a subject of current research. We postulate that the glycerol-water

dilutions of RM 8634 can be matched to a protein particle population by matching the mean particle image contrast of the diluted RM 8634 to that of the actual protein particles.
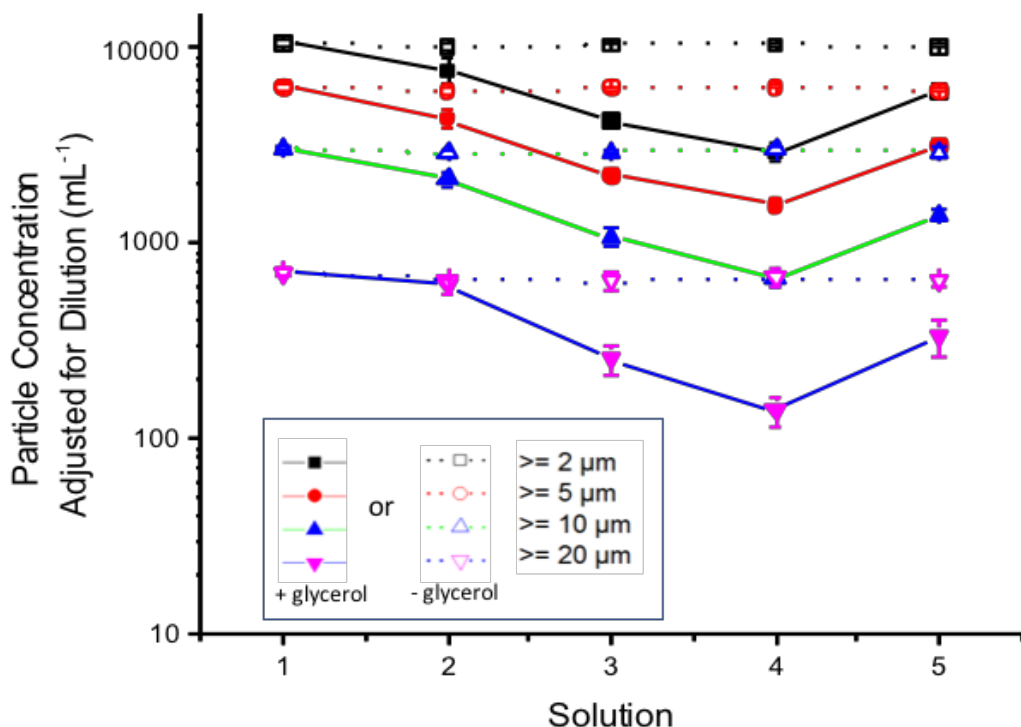
Figure 15. Reduction in apparent ETFE particle concentration on addition of glycerol to RM 8634. A) The solid lines represent solutions prepared with RM 8634 and 80 % glycerol solution (labeled "+ glycerol"). The dotted lines represent the corresponding solutions prepared with RM 8634 and 0.02% Triton X-100 solution (labeled "- glycerol"). Particle concentrations were corrected for dilutions. Each data point is the average of three separate measurements with the error bars representing one SD.

10. Using RM 8634 in Light Obscuration Particle Counters

LO particle counters can give erroneous readings when two or more particles in the detection orifice are counted as one. The differences between observed and actual particle count due to this effect are termed coincidence errors. With a polydisperse PSD, it is possible that the large numbers of particles smaller than the minimum reported size can introduce coincidence errors larger than predicted from studies of monodisperse microspheres.

To assess this effect for RM 8634, we produced another lot of ETFE by the same method as RM 8634 but at significantly higher number concentration. The formulation and ETFE abrasion methods were the same as for RM 8634. Three precleaned, 30 mL PETG vials were filled with the resulting lot. Each vial was measured five times on a PAMAS SVCC light obscuration instrument that had been highly characterized previously [2] to obtain the

37

apparent LO number concentration, N_{LO}. The vials were then diluted by addition of diluent and the measurements continued. The measurement and dilution process were continued up to eight-fold dilution.

Data were normalized by first multiplying by the dilution factor *DF*, and then dividing by the extrapolated *DF*-corrected number concentration corresponding to infinite dilution. If the coincidence error is negligible, data normalized in this manner will have a value of one. Manufacturers of commercial LO counters typically specify a number concentration $N_{10\,\%}$ above which the coincidence error is greater than 10 %. User determination of the coincidence error may give more accurate values of $N_{10\,\%}$ for a specific instrument [2]. Figure 16 shows the normalized number concentration versus the actual number concentration divided by $N_{10\,\%}$. We present the results as normalized to $N_{10\,\%}$ to account for large differences in $N_{10\,\%}$ among different LO instruments.

As number concentration increases, the coincidence error also increases, as seen for the data in Figure 16. The solid line shows the coincidence error predicted from previous measurements of monodisperse 4 µm microspheres in the same instrument. LO data for ETFE particles shown for two different size bins (≥ 1 µm and ≥ 4 µm) demonstrate similar behavior. The dashed black line is a coincidence error model [2] fit to the $N_{LO}(d_{rep,LO} \geq 1$ µm) data. The steeper slope of the dashed line relative to the solid black line indicates that the polydisperse ETFE particles have a coincidence error a factor of 1.4 larger than the microspheres. The greater error likely results from the effect of particles below 1 µm perturbing the optical signal in the instrument and possibly the irregular morphology of the ETFE particles.

From these results, we conclude that for our LO particle counter, coincidence errors are 10 % or less provided that the ETFE number concentration does not exceed $N_{10\%}/1.4 = 0.70\,N_{10\%}$ for the smallest diameter value of interest. The response of other LO instruments is likely similar, but the exact value of the coincidence error will vary depending on the instrument optical geometry.
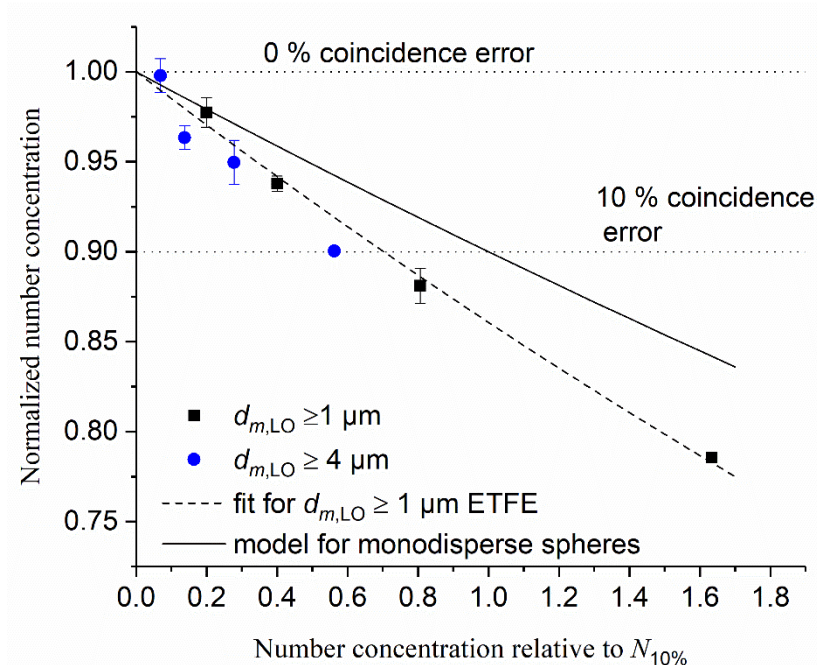
Figure 16. Coincidence effects in an LO particle counter. Measured number concentration normalized by the value extrapolated to zero number concentration, as a function of number concentration divided by $N_{10\%}$ for monodisperse spheres (blue dots and black squares for two size bins of ETFE particles). The deviation of the solid line from unity shows the coincidence error expected from studies of monodisperse, 4 µm microspheres on the same system. The dashed line is a fit to the $d_{\text{rep,LO}} \geq 1$ µm data of a coincidence-error model. Uncertainty bars are the standard uncertainty of the mean for three replicates.

11. Number Concentration Measurements of High-Density Particles

11.1. General Principles

Both protein particles and polystyrene microspheres have densities close to water. Fluorinated polymer particles (such as the RM 8634 ETFE particles), and potentially other particles of interest, are significantly denser than water. When a sample is loaded into a particle counting system, the particles begin settling. With time, the bottom of the sample will have a higher proportion of particles than the top, leading to inaccurate particle counts. This section describes protocols for the accurate measurement of the ETFE particle number concentration; the protocols described may be useful for other types of high-density particles.

The sedimentation velocity v_s is proportional to the density difference between the particle and its matrix fluid, $\Delta\rho$, and to the square of the particle diameter, d. As a result, large, high density particles sediment much faster than smaller, low density particles. Table 7 below gives the calculated time for solid spheres of a given size and composition to settle by 1 cm (a value large enough to significantly perturb counts in typical particle counters).

There are four methods for reducing the effects of sedimentation:

39

1. Stir the sample continuously. This is practical only with large-volume samples and counters equipped with stirrers.
2. Perform the measurement rapidly. If the measurement is completed quickly enough, the sedimentation will not affect the particle density, especially if the sampling system is configured to draw out fluid from the middle of the sample.
3. Measure the entire sample. Sedimentation only causes a redistribution of particles, and not an actual change in the particle numbers. If the entire sedimented sample is measured, the total number of particles will be unaffected.
4. Increase the viscosity of the matrix fluid. This method is not advised because viscosity modifiers can alter the refractive index of the matrix fluid and may also increase the number of unintentional particles and entrapped air bubbles.

Table 7. Calculated sedimentation times for spheres of the indicated diameter and material.

Material	Polystyrene	PMMA	ETFE	Silica	Soda-lime glass
Diameter			Time to sediment 1 cm		
(µm)			(min)		
1	5429	1572	409	174	191
2	1357	393	102	44	48
5	217	63	16	7	8
10	54	16	4	1.7	1.9
25	9	3	0.7	0.3	0.3
40	3	1.0	0.3	0.11	0.12
70	1.1	0.3	0.08	0.04	0.04

In practice, Method 2 (rapid measurements) works well with light obscuration particle counters and Method 3 (measure the whole sample) works well with flow imaging instruments. Details are provided below, but there are many other ways to achieve the same goal; i.e., suggestions below are not meant to be prescriptive.

11.2. **Light Obscuration Counters**

Typical sampling rates of light obscuration counters are 10 mL/min. This rate is sufficiently fast to mitigate the effects of sedimentation provided the following guidelines are followed:

a. Adjust the sampling needle to draw from the middle of the sample when possible.
b. Measure small volumes. It is preferable to measure no more than one or two milliliters before repeating steps c and d.
c. Gently tip the sample approximately 10× immediately prior to inserting the sample into the instrument.
d. Insert the sample just before beginning the actual measurement (i.e., do not place the sample in the instrument prior to choosing a method and assigning a file for data storage).

Stirring can also be effective. Possible downsides for using a stirrer are that the stirrer rubbing against the container walls can create particles, the stir bar must be very clean, and

the stirring may not be effective in raising very large particles from the bottom of the sampling chamber.

11.3. Flow Imaging Instruments

Flow imaging instruments have much slower sampling speeds compared to light obscuration, so rapid measurements are not practical. It is effective to set up the instrument method so that the instrument measures the whole sample. Although this sounds simple, complications arise due to the different ways instruments handle fluid priming. Two sample protocols are given below; either will suffice to give measurements with good repeatability. In addition to working with samples prone to sedimentation, these methods are useful when the sample volumes are limited. The examples given have been applied to commercial FI instruments. The user is recommended to follow the manufacturer's guidelines to first ensure that the instrument is clean and gives a clean baseline prior to running any samples.

11.3.1. Method for Instruments Loaded by Inserting a Filled Pipette Tip

The protocol is set up to start a measurement with the inlet tube filled with particle free fluid, and end with no more than 10 µL (0.01 mL) left in the inlet tube at the end of the measurement. This method requires correcting final results for dilution, but has the advantage that any large, rapidly sedimenting particles are counted. The load volume is chosen so that the run ends with only a small volume of the sample above the imaged portion of the flow cell. Ending with the meniscus near the flow cell helps to free particles adsorbed onto the walls of the tubing back into the sample of analyzed fluid. The following protocols are for manually filled instruments. For robotic instruments, protocols should be set up to prime 0.2 mL after stirring, followed by a single measurement of 0.2 mL (repeat as needed to accumulate more counts).

1. Determine the volume held in the tubing between the sample pipette tip and the imaged portion of the flow cell. To do this, first prime with water for 30 s and leave a bead of water on the adapter. Then, insert an empty pipette tip into the inlet using a pipette so that excess liquid overflows the adaptor instead of going up into the pipette tip. The volume of water remaining can be determined by setting the pump to a known flow rate and multiplying by the time for the meniscus to just appear in the camera view. The result obtained is the hold-up volume of the inlet tube, V_h.

2. Set up a method with zero prime volume, and a total volume of V_t.

3. Calculate the actual sample volume, $V_s = (V_t + 0.01 \text{ mL} - V_h)$. The 0.01 mL is the approximate volume of liquid left above the flow cell at the end of the run.

4. Prime the system with filtered liquid of the same composition as the matrix liquid of the actual sample and conduct any instrument optimization with the same liquid. (If the matrix liquid is water with a relatively low concentration of buffer and surfactant, the 'filtered liquid' can be simply 1 mL of particle-free water.)

5. Remove the tip. If you remove the tip slowly, the fluid remaining in the pipette will partially drain into the metal adaptor, leaving a "dome" of fluid on the inlet that eliminates bubbles and minimizes particles from plastic rubbing on plastic.

6. Tip the test sample 10× to mix and withdraw by a clean pipette from the center of the sample vial as quickly as possible.

7. Insert the pipette containing the sample into the sample inlet and initiate the sample measurement with zero prime volume.

8. If the determination of V_h was correct, the run will terminate with the fluid meniscus a short distance above the flow cell. If the meniscus passes through the cell prior to run termination, decrease V_h, or if the meniscus is high above the cell, increase V_h. Then recalculate V_s.

9. Adjust the reported number concentration by multiplying the reported particle concentration by the ratio (all liquid imaged)/(amount of sample pumped through) = (V_s + V_h – 0.01 mL)/(V_s – 0.01 mL).

10. Between each run, run 2 mL of clean liquid through the instrument.

11.3.2. Method for FI Instruments with a Fixed Inlet

The protocol is set up to start a measurement with the inlet tube filled with particle free fluid, measure the sample, rinse the tubing with a volume of particle-free liquid, and then terminate at the same liquid level as at the start.

1. Insert a clean pipette tip into the inlet. With a permanent pen, place a mark on the pipette tip just high enough so that if you add extra liquid to the pipette tip, there will be no trapped air bubble, which can give incorrect particle concentration measurements in the next run.

2. Fill the pipette with water and prime the system until the particle-free liquid is at the level of the pen mark. You will need to determine the amount of fluid held up between the pen mark and the imaged area of the flow cell, V_h. This can be done by stepwise drawing known volumes through the system and finding a volume just before the meniscus appears in the image.

3. If the instrument performs a background calibration separately after the method begins, determine the amount of fluid used during the background calibration. On a trial run, time the interval between starting a run and the counting of the first particle. Multiply the interval by the pump speed to obtain the volume used by the background calibration, V_b.

4. Set up a method with manual termination and no priming.

5. Fill the inlet tip with 1 mL of filtered liquid of the same composition as the matrix liquid of the actual sample. (If the matrix liquid is water with a relatively low concentration of buffer and surfactant, the 'filtered liquid' can be simply particle-free water.)

6. Prime the system until the particle-free liquid is at the level of the pen mark and set up the measurement.

7. Tip the test sample 10× to mix, and withdraw a volume V_s (e.g., 0.5 mL) from the center of the sample as quickly as possible.

8. Dispense the sample into the inlet pipette tip and start the measurement.

9. Manually terminate the run when the liquid meniscus is just above the flow cell (approximately 0.01 mL left in the tubing and cell on termination).

10. The reported number concentrations need to be adjusted to account for dilution. Multiply the reported particle concentration by the ratio (all liquid imaged)/(amount of sample pumped through) = (V_s + V_h – V_b – 0.01 mL)/(V_s – 0.01 mL).

Acknowledgments

References

1. Beers JS, Penzes WB (1999) The NIST length scale interferometer. *Journal of Research of the National Institute of Standards and Technology* 104(3):225-252.

2. Ripple DC, DeRose PC (2018) Primary Determination of Particle Number Concentration with Light Obscuration and Dynamic Imaging Particle Counters. *Journal of Research of the National Institute of Standards and Technology* 123:123002.

3. French RH, Rodriguez-Parada JM, Yang MK, Derryberry RA, Lemon MF, Brown MJ, Haeger CR, Samuels SL, Romano EC, Richardson RE (2009) *Optical Properties of Materials for Concentrator Photovoltaic Systems*. 2009 34th IEEE Photovoltaic Specialists Conference, Vols 1-3:149-154.

4. Cavicchi RE, King J, Ripple DC (2018) Measurement of Average Aggregate Density by Sedimentation and Brownian Motion Analysis. *Journal of Pharmaceutical Sciences* 107(5):1304-1312.

5. Myers KJ, Reeder MF, Fasano JB (2002) Optimize mixing by using the proper baffles. *Chemical Engineering Progress* 98(2):42-47.

6. Lettieri TR, Hartman AW, Hembree GG, Marx E (1991) Certification of SRM 1960 - Nominal 10 µm Diameter Polystyrene Spheres (Space Beads). *Journal of Research of the National Institute of Standards and Technology* 96(6):669-691.

7. Welcome to Python.org. https://www.python.org/.

8. International Organization for Standardization (2004) ISO 13322-1. Particle size analysis — Image analysis methods — Part 1: Static image analysis methods. (International Organization for Standardization, Genève, Switzerland).

9. Saffman PG (1965) Lift on a Small Sphere in a Slow Shear Flow. *Journal of Fluid Mechanics* 22:385-400.

10. Asmolov ES, Dubov AL, Nizkaya TV, Harting J, Vinogradova OI (2018) Inertial focusing of finite-size particles in microchannels. *Journal of Fluid Mechanics* 840:613-630.

11. Krishnan GP, Leighton DT (1995) Inertial Lift on a Moving Sphere in Contact with a Plane Wall in a Shear-Flow. *Physics of Fluids* 7(11):2538-2545.

12. International Organization for Standardization (2008) ISO 9276-6. Representation of results of particle size analysis - Description and quantitative representation of particle shape and morphology. (International Organization for Standardization, Genève, Switzerland).

13. Ritchie N, Filip V (2011) SEMantics for High Speed Automated Particle Analysis by SEM/EDX. *Microscopy and Microanalysis* 17(S2):896-897.

14. Newbury DE, Ritchie NWM (2015) Performing elemental microanalysis with high accuracy and high precision by scanning electron microscopy/silicon drift detector

energy-dispersive X-ray spectrometry (SEM/SDD-EDS). *Journal of Materials Science* 50(2):493-518.

15. International Bureau of Weights and Measures, International Organization for Standardization (1993) *Guide to the expression of uncertainty in measurement* (International Organization for Standardization, Genève, Switzerland), 1st Ed., pp viii–101.

Appendix A: Optical Microscope Biases

A.1 Background
The limited spatial resolution and depth of field of optical microscopes introduces errors in the determination of the effective diameter of each particle. When an irregular object of low refractive index contrast is measured in a microscope with low optical resolution, regions of low image intensity may erode following thresholding, leading to reduced apparent diameter. However, if the particle has a convoluted shape and the image border is expanded due to diffraction effects, the increase in apparent diameter can be larger than for a sphere. On consideration of these two effects, we chose not to calibrate the FI or SFM with microspheres alone. In calibrating the FI for diameter, our basic approach was to modify a commercial upright optical microscope to mimic the optics of the FI. Measurements of a set of PMMA microspheres of known diameter on both the FI and the optical microscope confirmed that the difference between uncorrected image diameters and known diameters was equivalent for both instruments provided we multiplied the optical-microscope difference by a factor $C_d = 1.11$. We assumed that the C_d correction would apply to measurements of the ETFE particles as well. Then, individual ETFE particles could be measured at a low-resolution configuration (mimicking the FI) and in a high-resolution configuration ($40\times$, 0.55 NA). Even the high-resolution objective has limited optical resolution, which we corrected to obtain the estimated actual ETFE particle diameter. From a set of these low- and high-resolution diameters, we fit a model function for the difference between the low-resolution measured diameter and the apparent true diameter. That function, multiplied by C_d, was subtracted from the uncorrected FI image diameters to obtain the actual ETFE particle diameters.

The development of a model for the SFM was similar, but required only modification of the light source to match the SFM. (The PC measurements were done on an optical microscope under similar conditions to the SFM calibration measurements and needed no additional configuration adjustments.)

An upright optical microscope (model DMR, Leica Microsystems, Inc., Buffalo Grove, IL) equipped with a Lumenera Model Infinity2-2M 2.0 Megapixel Microscopy CCD Camera (Lumenera Corporation, Ottawa, ON, Canada) was used for the measurements. Image pixel size was determined daily by measurement of a NIST-calibrated stage micrometer.

The dependence of particle diameter on various settings was assessed using a variety of microspheres of the following materials and diameters: PMMA (1, 3, 5, 10, 20, and 70) μm

44

and PSL 4.993 µm and silica (2.14 and 2.56) µm. ETFE particles used were from a highly concentrated stock, approximately 300× higher than RM 8634.

Since the optical microscope measurements were time-consuming and it was critical to measure the same particle for each optical configuration, particles were immobilized in gelatin prior to imaging. A 0.04 % mass concentration solution of gelatin in deionized water was prepared and filtered through a 0.45 µm PVDF filter. Particle suspensions were combined with the gelatin solution at 0.025% mass concentration gelatin, pipetted onto clean glass slides, and covered with a cover slip. The edges of the cover slip were sealed using red, solvent-based nail polish to prevent evaporation.

A.2 Calibration Curve for the FI

The first step was to configure the optical microscope 5× setting to approximate the optical configuration of the FI. This required physical modification of the 5× objective numerical aperture (NA_{obj}), matching the collection light wavelength, and determination of the best numerical aperture for illumination (NA_{ill}).

To adjust NA_{obj}, a preliminary assessment was performed by collecting images of microspheres on the optical microscope 5× setting and the FI (4×). (The standard Leica objectives are 5× and not 4×; the NA_{obj} is more critical than the objective magnification.) The microsphere diameters of the uncorrected images were compared and used to estimate the reduction of NA_{obj} needed to bring the diameters into close agreement after nominally accounting for differences in magnification and camera pixel size. A smaller aperture was fabricated from a blackened orifice and glued on top of the existing back-focal-plane aperture of the optical microscope 5× objective.

The setting of NA_{ill} has an effect on contrast and diffraction, thus affecting the size determination of the particles in the images. To match NA_{ill} of the optical microscope with the 5× objective to that of the FI, slides were prepared with both polystyrene (4.993 µm diameter) and silica (2.14 µm and 2.56 µm diameters) microspheres. These two materials have significantly different indices of refraction (1.43 for silica microspheres and 1.59 for polystyrene) and will behave differently when imaged in terms of contrast. We collected images of the particles on these slides at a range of NA_{ill}. Images of these microspheres in water were also obtained on the FI. For each particle, as a measure of contrast, we calculated the integrated difference in image intensity ΔI between the particle and the background. The values of ΔI include normalization to the image pixel size and background intensity. Also, minor corrections were applied to account for the difference in the refractive index (n) of the medium containing the particles. A value of NA_{ill} was determined by matching the upright optical microscope ΔI to the FI value of ΔI. Note that this correction is purely empirical—we did not attempt to replicate the exact illumination source and geometry of the FI. Final corrections were applied to the calibration (see below) to account for imperfections in matching of the methods.

Filter glasses and emission filters were used to match the illumination and collection wavelengths of the FI instrument. In addition, we confirmed that the particle contrast varied

quite slowly over a large range of focal positions with a maximum that was within the optimal contrast position focusing done manually by visual inspection.

After configuration of the optical microscope to mimic the output of the FI, images of PMMA microspheres in gelatin on microscope slides were collected on both 5× and 40× settings of the optical microscope. The diameter of the microspheres had been previously determined using the center-finding method [6] for at least 100 microspheres from each lot. The same microsphere mixtures used for the calibration curves were diluted roughly by a factor of 10 and measured on the FI. We found that the reported FI results could be closely duplicated in an ImageJ analysis of the raw FI images by using a threshold of 4 % difference from the median intensity and performing a single binary fill operation. (These steps were incorporated into an ImageJ macro.) Particles were discarded if they appeared to be merged with another particle or any sample contamination or if they appear to be other than microspheres. Particle areas were converted into an equivalent circular diameter (d_m) in pixels. This d_m value (in pixels) was then converted to d_m in units of micrometers using the calibrated pixel size.

Once the microsphere calibration curve was made, data was collected in a similar fashion using ETFE. For the 40× magnification, an image stack was taken for each particle, since the full perimeter was not in focus for any one image. This stack was analyzed in ImageJ to look for particles that lost area, especially interior area, or broke into pieces in the 4 % threshold. The particles that fit these criteria were reanalyzed by hand-drawing a perimeter of the particle to include areas that may have been lost or to connect particles that may have broken up. This hand-drawn perimeter was then used as the perimeter of the particle, and the same particle statistics are calculated as in the case of the auto-analysis.

A.3 Calibration Curve for the SFM

To configure the upright optical microscope, a light source identical to the one used on the SFM was fitted to the optical microscope. Both upright optical and SFM condensers were adjusted for Köhler illumination, and objective lenses had identical numerical apertures. To fill the upright optical microscope illumination aperture at 40×, we needed to modify the light source by focusing the beam through a tight aperture and then collimating prior to light entry into the microscope. Because the SFM microscope is inverted (light source comes from above) the particles are all settled against a single plane on the objective side of the slide. To correct for this on the upright microscope (not inverted), slides were prepared using slightly lower concentrations of gelatin (to allow particles to settle prior to setting of the gelatin) and allowed to gel in an upside-down orientation so the particles can settle in a plane against the cover slip. When imaged on the upright microscope, all the particles were settled against the cover slip. The particles were focused by locating the focal position where the 1 µm particles were just changing from light interior to dark and then rotating the focus knob 6 µm in the direction of darker particle. This is the same procedure used during SFM measurements.

Once the upright optical microscope light source and slide preparation were set to mimic the SFM settings, images were collected of PMMA microspheres of (1, 3, 5, 10, and 20) µm on both the 10× and 40× magnification settings as described above. Data for the SFM calibration curve with microspheres was analyzed in a similar manner as above for the FI

46

calibration curve microsphere measurements.   ImageJ software was used for analysis of both the $10\times$ and $40\times$ microsphere measurements, using zero dilate/erode steps and auto edge detection with a threshold of 4 %. Particle areas were then converted to d_m in pixels and then to d_m in micrometers using the calibrated stage micrometer measurements.

A.4 Final Corrections to the FI and SFM Calibration Curves

In this section, we describe how the PSD data sets described above were mathematically combined to create quantitative values for the difference between measured (d_m) and actual (d_a) particle diameters for the FI (Δd_{FI}) and SFM/PC ($\Delta d_{10\times}$). The actual diameter is known initially only for the PMMA microspheres, for which the center-distance-finding method gave diameters d_{CDF} equal to the actual diameter.

For greater clarity, we describe the procedure for the FI; a similar procedure is used for the SFM/PC. Ideally, the measured diameter on the optical microscope $d_{m,5\times}$ would be equivalent to the measured diameter of the FI, d_{FI}, and the high-resolution measured diameter would be a good approximation to the actual diameter. There are, in fact, two complications. First, the adjustment of the optical microscope to mimic the FI is imperfect. We compensate by multiplying the diffraction correction obtained at $5\times$ by a fixed factor C_d to obtain the diffraction correction for the FI. C_d is determined by examining data for PMMA microspheres with known diameter d_{CDF}. Second, the high-resolution images at $40\times$ still have appreciable diffraction error, so that $d_{m,40\times}$ is not equal to d_a. We use theoretical estimates and experimental observations to obtain the ratio of diffraction corrections at $5\times$ and $40\times$: $\Delta d_{5\times}/\Delta d_{40\times}$. Then, $\Delta d_{5\times}$ is modeled as a function of the actual diameter d_a. For ETFE, the actual diameter is not directly measured, but knowledge of the ratio $\Delta d_{5\times}/\Delta d_{40\times}$, the correction factor C_d determined using microspheres, and the combined data for $d_{m,5\times}$ vs. $d_{m,40\times}$ provide sufficient information to fit the model parameters. The details of the analysis follow.

The analysis involves manipulation of several diameters and diameter differences. All diameters represent equivalent circular diameters. Here are symbols and definitions for the terms used:

d_{CDF}	Diameter of microspheres determined by the center-distance finding method
d_a	Actual particle diameter, equal to d_{CDF} for microspheres and d (defined above in the Glossary) for ETFE
d_{rep}	Particle diameter reported by the FI, confirmed to be equivalent to d_a within measurement uncertainty for microspheres
$d_{m,5\times}$, $d_{m,10\times}$, $d_{m,40\times}$	Measured, uncorrected particle diameter in the optical microscope with modified-$5\times$, $10\times$, or $40\times$ objectives, respectively
$d_{m,\text{FI}}$, $d_{m,\text{SFM}}$, $d_{m,\text{PC}}$	Measured, uncorrected particle diameter of the raw images in the FI, SFM, or PC instrument, respectively

Δd_{FI}	For FI instrument images, difference between measured and actual particle diameters due to diffraction and other optical effects. Δd_{FI} equals $d_{m,\text{FI}} - d_{\text{rep}}$ for microspheres
$\Delta d_{5\times}$, $\Delta d_{10\times}$, $\Delta d_{40\times}$	Difference between measured and actual particle diameters due to diffraction and other optical effects, for optical microscope with modified 5×, 10×, or 40× objective, respectively

We next used a set of PMMA microspheres for which we had previously determined their diameters independent of diffraction effects, d_{CDF}, using the center-distance-finding method. We examined the image diameter of these PMMA microspheres in the upright optical microscope using both the modified low-aperture 5× objective and a high-aperture 40× objective to determine $\Delta d_{5\times}$ and $\Delta d_{40\times}$, respectively. We created empirical models as a function of the actual diameter d_a (d_a is equivalent to d_{CDF} for the microspheres) for both $\Delta d_{5\times}$ and $\Delta d_{40\times}/\Delta d_{5\times}$. The diffraction correction for the 5× objective, $\Delta d_{5\times}$, was represented by the empirically determined function

$$\Delta d_{5\times} = g\left(d_a\right) = a_0 \frac{\left(1 + a_1 \ln\left(d_a\right) + a_2 \ln\left(d_a\right)^2\right)}{1 + \left(a_3/d_a\right)^{a_4}} \quad , \tag{22}$$

where a_0, a_1, a_2, a_3, and a_4 are all constants.

Equation 22 represents the diffraction errors encountered in the optical microscope used to generate the FI correction curve, but may not represent the errors encountered in the FI if the optical microscope adjustment was not equivalent to the FI. To assess the equivalence, we compared values of Δd for both the optical microscope and FI as a function of d_{CDF} (see Figure 17 below). Raw FI images were analyzed with ImageJ to obtain measured diameters $d_{m,\text{FI}}$, from which instrument-reported diameters d_{rep} were subtracted to obtain experimental values of Δd_{FI}. Note that d_{rep} is confirmed to be equivalent to d_a within measurement uncertainty for these microspheres. We found that the optical microscope values of $\Delta d_{5\times}$ needed to be increased by 11 % ($C_d = 1.11$) to give a good match to the FI values:

$$\Delta d_{\text{FI}} = C_d \Delta d_{5\times} = C_d\, g(d_a) \,. \tag{23}$$

Next, the corrections for ETFE particle measurements were considered. Measurements of ETFE particles at both 5× and 40× magnifications were obtained on the upright optical microscope, and the results plotted as ($\Delta d_{5\times} - \Delta d_{40\times}$) vs. $d_{m,40\times}$ (not shown). As with the microspheres, the analysis proceeded by assuming a functional form for $\Delta d_{5\times}$ as a function of d_a, where $\Delta d_{5\times} = h(d_a) = b_0 + b_1\ln(d_a)$. For microspheres that were of approximately the same refractive index mismatch with the fluid as ETFE, the ratio $\Delta d_{40\times}/\Delta d_{5\times}$ is close to the theoretical value of 0.13 obtained from the ratio of objective numerical apertures. Assuming that $\Delta d_{40\times}/\Delta d_{5\times} = 0.13$ and that Eq. 23 is valid for ETFE, the model parameters were adjusted so that the calculated model values of ($\Delta d_{5\times} - \Delta d_{40\times}$) vs. $d_{m,40\times}$ fit the data. Figure 18 shows the data obtained for the measured diameter $d_{m,5\text{x}}$ versus $d_{m,40\times}$ and the model fitted to the data.

To use the resulting expression for $\Delta d_{\text{FI}} = C_d\, h(d_a)$, we needed to find the correspondence between the reported diameter values for the FI, d_{rep}, and the actual diameter of an ETFE

48

particle, d_a. To obtain this relation, note that the reported FI value (d_{rep}) has a correction for spheres subtracted by the instrument software. The raw image diameter, $d_{m,FI}$, for ETFE is obtained by adding back the diffraction correction for spheres $C_d\, g\, (d_{rep})$ to d_{rep}. Alternatively, $d_{m,FI}$ is also equal to the actual ETFE diameter plus the diffraction term determined above: $d_{m,FI} = d_a + \Delta d_{FI} = d_a + C_d h(d_a)$. Equating these two approaches:

$$d_{rep} + C_d\, g\left(d_{rep}\right) = d_a + C_d\, h(d_a) , \tag{24}$$

where the left side of Eq. 24 is the measured diameter for the FI instrument, and the right side is the measured diameter for the optical microscope after scaling to match the FI. Eq. 24 can be solved iteratively using Newton's method to find the root of the function

$$S(d_a) = d_{rep} + C_d\, g\,(d_{rep}) - [d_a + C_d\, h(d_a)] \quad . \tag{25}$$

For every value of d_a desired for the final compilation of the PSD (e.g., 10.00 µm), the root of Eq. 25 gives the corresponding d_{rep} value. The exported particle count data from the FI were sorted into bins using these corresponding d_{rep} values as size limits. The generation of PSD histograms by this process (see Section 5.1) was performed with spreadsheet templates.

Analysis of the SFM diameter corrections proceeded in the same manner as for the FI, except that the ETFE data was obtained using a 10×, $NA = 0.30$ objective with a 470 nm LED light source. Application of the resulting function for $\Delta d_{10\times}$ (using the same functional form as for $\Delta d_{5\times}$) was easier for the SFM than for the FI because the ImageJ analysis gave a direct report of $d_{m,10\times}$. Results for the measured diameter at the same magnification as the SFM, $d_{m,10\times}$, versus $d_{m,40\times}$ are shown in Figure 19. The difference $\Delta d_{10\times}$ was applied by finding the measured diameter that corresponded to the actual diameter values chosen for the final data compilation. Correction to the actual diameter simply consisted of finding $d_a = d_{m,10\times} - \Delta d_{10\times}$. The spreadsheet templates for generating PSD histograms determined particle concentrations according to the size bins of $d_{m,10\times}$ that corresponded to the desired d_a.
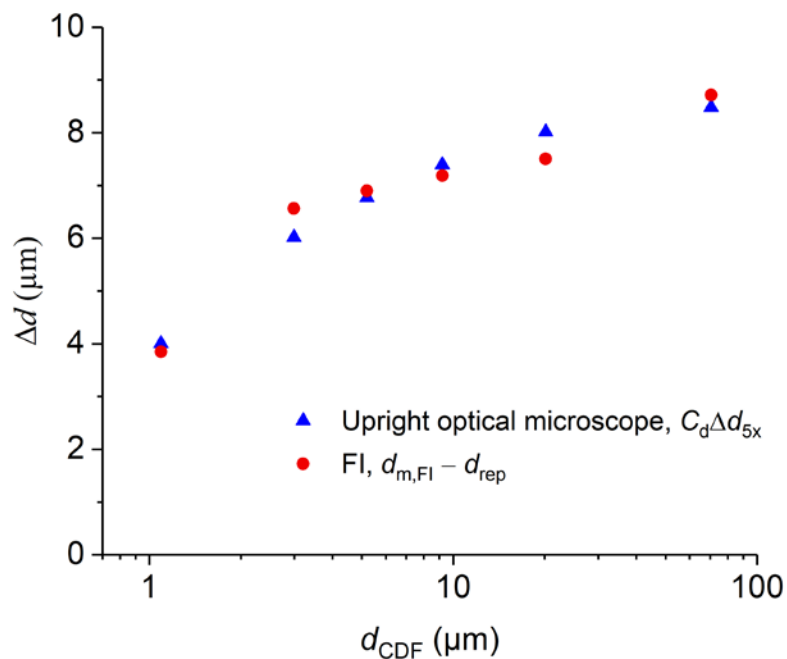
Figure 17. Correction Δd for both the adjusted optical microscope data and the FI, for PMMA microspheres.
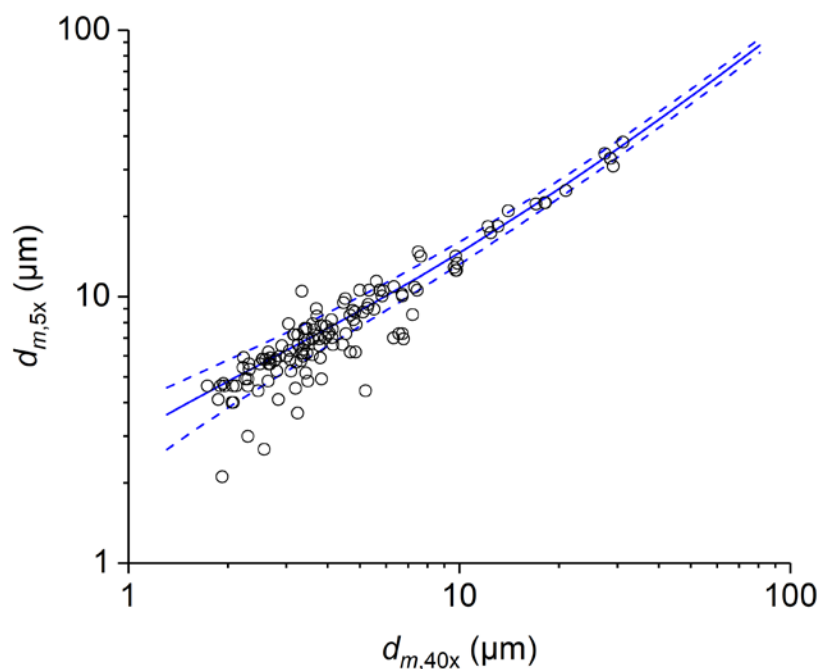

Figure 18. Measured diameter for ETFE at 5× versus measured diameter at 40× (circles) data; (solid line) model based on $\Delta d_{5x} = h(d_a) = b_0 + b_1 \ln(d_a)$; (dashed lines) model ± combined standard uncertainty u_c.

50
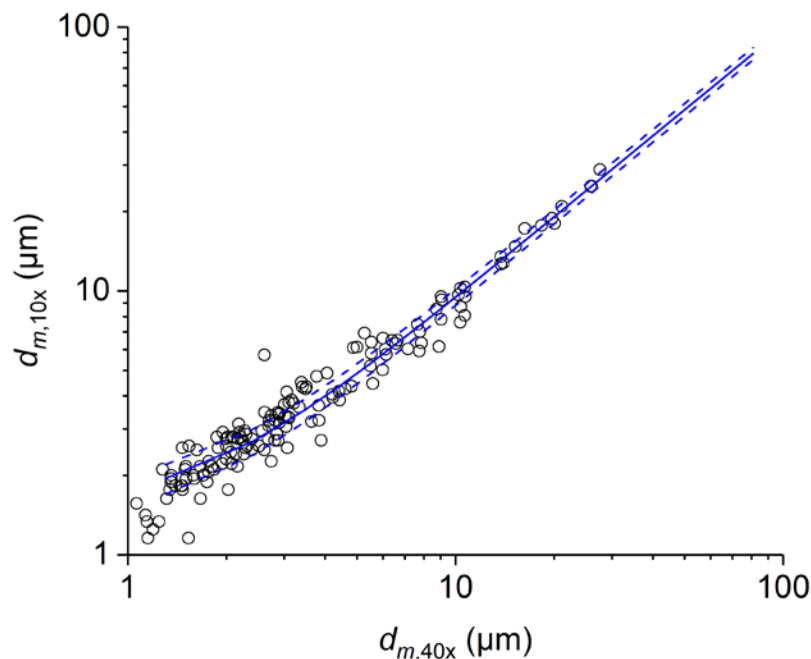
Figure 19. Measured diameter for ETFE at 10× versus measured diameter at 40× (circles) data; (solid line) model based on $\Delta d_{10\times} = h(d_a) = b_0 + b_1 \ln(d_a)$; (dashed lines) model $\pm u_c$.

Appendix B: Summary Tables of PSD Biases and Uncertainty

While the largest uncertainties associated with each technique were discussed in the respective sections above, a summary of all uncertainties and known biases associated with the PSD measurements (FI, SFM, and PC) are tabulated below in Tables 8 to 11. Uncertainties are expressed as standard uncertainties. Type A uncertainties are those determined by statistical methods: Type B uncertainties are determined by non-statistical methods [15].

Table 8 lists uncertainties that are common to all three methods. In addition to lot homogeneity and stability (determined by FI), we discovered that PFA particles were created by repeated opening and closing of the vials. When ten vials containing diluent alone (no ETFE) were intentionally opened and closed multiple times (20 open/close/tip cycles), the mean combined uncertainty in particle concentration ranged from 1.5 % for the smaller size limits (up to 7 µm), and rising to 3.4 % for $d_a \geq 20$ µm and 6.8 % for $d_a \geq 30$ µm.

There is an additional uncertainty in particle diameter that affects the full uncertainty of the PSD of a polydisperse material. All ETFE size measurements, for all three PSD measurement techniques, are correlated to diameter measurements of the ETFE using a 40×/0.55 NA objective upright optical microscope. The uncertainty of this correlation has two subcomponents: a) the uncertainty of the correlation between 10× (or 5×) and 40× effective diameter measurements, and b) the uncertainty of diffraction corrections made to adjust the 40× measurements to an estimate of true size. Studies of PMMA microspheres of known size, suspended in water/glycerol to mimic the low refractive index mismatch

51

between ETFE and water, were used to assess the accuracy of our estimates for the difference between the measured and actual ETFE diameters at 40×, Δd_{40}. These measurements showed good agreement between theoretical estimates of Δd_{40} and the observed difference between the measured and actual diameters of the PMMA microspheres. Actual ETFE, however, is more complex than the PMMA microspheres in two ways. First, because ETFE has a convoluted perimeter, expansion of the particle edge by a fixed distance will increase the apparent area of the ETFE by more than expansion of an equivalent sphere. This effect implies that Δd_{40} is larger than predicted by diffraction theory. Conversely, microspheres have uniformly dark perimeters compared to ETFE. Where ETFE is faint, the thresholded edge of the particle does not expand as much as predicted by diffraction, especially when the focus is optimized for contrast of the particle edges. Based on the measured morphology, the perimeter effect could plausibly lead to Δd_{40} being twice as large as the simple diffraction model. Based on an assessment of microsphere and ETFE particle diameters as a function of focus, effects due to contrast and focus could plausibly lead to $\Delta d_{40} \approx 0$. As a result, Δd_{40} was kept at the simple diffraction value, and the standard uncertainty for diameter was taken as $\Delta d_{40}/2$. Table 9 summarizes the uncertainty of the combined diffraction corrections that had to be applied to the optical images for FI, SFM, and PC measurements of ETFE particles.

In addition to the number concentration uncertainties that are the same for all methods, there are additional uncertainties in number concentration for each of the three methods used. For each method, Table 10 gives standard uncertainties at the different size bins. The uncertainty in the dilution factor (dilution due to priming) was obtained by examining variations in the amount of sample processed by the instrument), and then taking the corresponding variations in dilution factor as the assigned standard uncertainty. The convolution effects resulting in mis-assignment of particle diameter and consequent errors in the PSD are difficult to model, so the standard uncertainty of this effect was taken as equal to the magnitude of the correction itself. The end-of-run particles were assessed in multiple control experiments, but it is possible that these experiments undercounted particles that remained adherent on the tubing or that were obscured by the air bubble passing through the cell. The standard uncertainty as a function of diameter was obtained by plotting the ESDM for each size limit, fitting a trend line to that data, and then adding 20 % of the end-of-run correction as an estimate of possible uncounted particles. The uncertainty of the correction for unimaged particles at the edge of the flow cell was taken as the ESDM of the correction evaluated for eight FI runs. For all techniques, the cell thickness was inferred from FI, SFM, or PC measurements of PSL microsphere suspensions of known number concentration, accounting for the uncertainty of the assigned PSL number concentration. The standard uncertainty includes the ESDM of the microsphere measurements. The relative standard uncertainty due to background counts was negligible and was taken as the relative change in number concentration with and without the background counts subtracted from the ETFE particle counts. For the PC, the mean ESDM for number concentration for the two data-sets was assigned as the standard uncertainty for repeatability. For the SFM, as a measure of the imperfection of our assessment of the 20 µL runs, we include a relative uncertainty for sedimentation and flushing equal to the relative uncertainty of the difference in number concentration from image frames obtained just before and just after the 200 µL flush.

Inspection of Figure 9 (see Section 5.1) shows that the PC, SFM, and FI data sets have an approximate rank ordering of number concentration. This ordering is most likely due to

systematic differences between the three measurement methods, in either number concentration or diameter. An additional correlation of the data occurs because $N(d)$ for a particular value of d is partially dependent on the same particle counts used in the determination of $N(d)$ for larger values of d. For these reasons, the uncertainty obtained by a weighted-least-squares algorithm that presumes statistically independent data values is not appropriate.

Instead, we obtain the standard uncertainty for each d value, combining uncertainties as appropriate for finding the weighted values of $N(d)$ at each diameter and propagating the diameter uncertainties using the approximation $U(N) \approx N \cdot U(\ln N)$ and the Law of Propagation of Uncertainty. Expanded uncertainties $U(N)$ given in Table 1 are obtained by multiplying the combined standard uncertainties u_c by the coverage factor of $k = 2$. Values of $N \pm U(N)$ were each fit by a Weibull function to generate the $k = 2$ band shown in Figure 10.

Corrections for several of the effects on number concentration that have uncertainties supplied in Tables 8 to 10 also were applied to the data. These corrections are listed as multiplicative factors in Table 11. The measured number concentration was multiplied by the product of all factors, denoted C_N (distinct from the diameter prefactor C_d in Appendix A).

Table 8. Lot homogeneity, stability, and presence of thread debris, expressed as number-concentration relative standard uncertainties, $u_r(N)$.

Component	Type	Number concentration relative uncertainty, homogeneity and stability									
		$d \geq 1$ µm	$d \geq 2$ µm	$d \geq 3$ µm	$d \geq 5$ µm	$d \geq 7$ µm	$d \geq 10$ µm	$d \geq 15$ µm	$d \geq 20$ µm	$d \geq 25$ µm	$d \geq 30$ µm
Lot homogeneity	A	1.4 %	1.4 %	1.4 %	1.6 %	1.5 %	1.3 %	0.9 %	1.2 %	2.4 %	3.3 %
Stability	B	7.0 %	6.0 %	5.0 %	4.0 %	2.8 %	1.6 %	1.6 %	1.6 %	1.6 %	1.6 %
Thread debris	B	1.5 %	1.5 %	1.5 %	1.5 %	1.5 %	1.7 %	2.4 %	3.4 %	4.9 %	6.8 %
$u_r(N)$		7.3 %	6.3 %	5.4 %	4.6 %	3.5 %	2.7 %	3.0 %	4.0 %	5.7 %	7.7 %

Table 9. Summary of diameter uncertainty, expressed as standard uncertainties.

Component	Type	Diameter uncertainty (µm), FI measurements									
		$d \geq 1$ µm	$d \geq 2$ µm	$d \geq 3$ µm	$d \geq 5$ µm	$d \geq 7$ µm	$d \geq 10$ µm	$d \geq 15$ µm	$d \geq 20$ µm	$d \geq 25$ µm	$d \geq 30$ µm
Diffraction correction	B		0.92	0.93	0.97	1.01	1.09	1.26	1.26	1.26	1.26

Component	Type	Diameter uncertainty (µm), SFM measurements									
Diffraction correction	B	0.26	0.30	0.34	0.42	0.50	0.63	0.84	0.84	0.84	0.84

Component	Type	Diameter uncertainty (µm), PC measurements									
Diffraction correction	B	0.26	0.30	0.34	0.42	0.50	0.63	0.84	0.84	0.84	0.84

Table 10. Summary of number-concentration uncertainty for PSD measurements, expressed as relative standard uncertainties, $u_r(N)$.

Component	Type	$d \geq 1$ μm	$d \geq 2$ μm	$d \geq 3$ μm	$d \geq 5$ μm	$d \geq 7$ μm	$d \geq 10$ μm	$d \geq 15$ μm	$d \geq 20$ μm	$d \geq 25$ μm	$d \geq 30$ μm
				Number concentration relative uncertainty, FI measurement							
Cell constant	B		1.1 %	1.1 %	1.1 %	1.1 %	1.1 %	1.1 %	1.1 %	1.1 %	1.1 %
Convolution effects	B		2.3 %	2.0 %	4.2 %	4.2 %	2.5 %	1.5 %	0.9 %	0.7 %	1.2 %
Linearity	B		0.5 %	0.5 %	0.5 %	0.5 %	0.5 %	0.5 %	0.5 %	0.5 %	0.5 %
Priming dilution factor	B		0.4 %	0.4 %	0.4 %	0.4 %	0.4 %	0.4 %	0.4 %	0.4 %	0.4 %
Edge particles	B		0.1 %	0.1 %	0.1 %	0.1 %	0.2 %	0.3 %	0.5 %	0.6 %	0.8 %
End-of-run particles	B		0.5 %	0.6 %	0.7 %	0.9 %	1.0 %	1.2 %	1.5 %	2.0 %	2.0 %
Background	B		0.5 %	0.3 %	0.1 %	0.1 %	0.1 %	0.0 %	0.0 %	0.0 %	0.0 %
$u_r(N)$			2.7 %	2.5 %	4.4 %	4.5 %	3.0 %	2.3 %	2.2 %	2.5 %	2.8 %
				Number concentration relative uncertainty, SFM measurements							
Repeatability	A	2.1 %	2.4 %	2.2 %	2.2 %	2.8 %	4.5 %	7.2 %	7.2 %	7.8 %	9.3 %
Cell constant	B	1.1 %	1.1 %	1.1 %	1.1 %	1.1 %	1.1 %	1.1 %	1.1 %	1.1 %	1.1 %
RM vial/(2.5×, 5× vial) ratio	B	0.8 %	0.8 %	0.8 %	0.9 %	0.9 %	1.0 %	1.1 %	1.7 %	2.3 %	2.8 %
Linearity	B	3.5 %	3.6 %	3.9 %	5.0 %	6.7 %	10.7 %	3.3 %	3.3 %	3.3 %	3.3 %
Evaporation	B	0.8 %	0.8 %	0.8 %	0.8 %	0.8 %	0.8 %	0.8 %	0.8 %	0.8 %	0.8 %
Background	B	1.7 %	1.5 %	1.1 %	0.2 %	0.0 %	0.0 %	0.0 %	0.0 %	0.0 %	0.0 %
Sedimentation/flushing	B	3.0 %	5.0 %	5.0 %	5.0 %	4.0 %	3.0 %	1.0 %	1.0 %	1.0 %	1.0 %
$u_r(N)$		5.6 %	7.0 %	7.0 %	7.6 %	8.5 %	12.1 %	8.1 %	8.3 %	9.0 %	10.4 %
				Number concentration relative uncertainty, PC measurements							
Repeatability	A	3.8 %	4.0 %	4.3 %	4.3 %	5.8 %	7.6 %	12.5 %	20.6 %	23.4 %	20.1 %
Linearity	B	0.4 %	0.3 %	0.3 %	0.2 %	0.1 %	0.0 %	0.0 %	0.0 %	0.0 %	0.0 %
Cell constant	B	2.5 %	2.5 %	2.5 %	2.5 %	2.5 %	2.5 %	2.5 %	2.5 %	2.5 %	2.5 %
RM vial/(2.5×, 5× vial) ratio	B	0.8 %	0.8 %	0.8 %	0.9 %	0.9 %	1.0 %	1.1 %	1.7 %	2.3 %	2.8 %
Data selection	B	2.7 %	4.0 %	4.3 %	5.1 %	7.5 %	10.7 %	19.6 %	41.9 %	51.0 %	29.0 %
Threshold difference	B	0.2 %	0.4 %	0.7 %	0.6 %	2.4 %	2.5 %	1.2 %	2.9 %	4.7 %	4.1 %
Background counts	B	0.9 %	0.6 %	0.3 %	0.0 %	0.0 %	0.0 %	0.0 %	0.0 %	0.0 %	0.0 %
$u_r(N)$		5.4 %	6.3 %	6.7 %	7.2 %	10.1 %	13.6 %	23.5 %	46.8 %	56.4 %	35.7 %

Table 11. Summary of number-concentration bias for PSD measurements, expressed as a number-concentration prefactor C_N that is multiplied with the measured $N(d)$ to obtain the corrected value of $N(d)$. Each C_N value is obtained by multiplying factors for each component.

	Number concentration bias factor, FI measurement								
Component	$d \geq 2$ µm	$d \geq 3$ µm	$d \geq 5$ µm	$d \geq 7$ µm	$d \geq 10$ µm	$d \geq 15$ µm	$d \geq 20$ µm	$d \geq 25$ µm	$d \geq 30$ µm
Convolution effects	1.023	1.020	0.958	0.958	0.975	0.985	0.991	0.993	0.988
Edge particles	1.000	1.004	1.007	1.008	1.008	1.010	1.014	1.017	1.018
End-of-run particles	1.000	1.004	1.007	1.016	1.024	1.040	1.054	1.065	1.075
C_N	1.023	1.028	0.971	0.981	1.006	1.035	1.059	1.076	1.081

	Number concentration bias factor, SFM measurements									
Component	$d \geq 1$ µm	$d \geq 2$ µm	$d \geq 3$ µm	$d \geq 5$ µm	$d \geq 7$ µm	$d \geq 10$ µm	$d \geq 15$ µm	$d \geq 20$ µm	$d \geq 25$ µm	$d \geq 30$ µm
RM vial to (2.5×, 5× vial) ratio	1.022	1.022	1.019	1.011	1.009	1.015	1.025	1.047	1.054	1.077
Linearity	1.011	1.015	1.021	1.038	1.058	1.102	1.000	1.000	1.000	1.000
Sedimentation	1.022	1.001	1.000	1.000	1.000	1.000	1.000	1.000	1.000	1.000
C_N	1.056	1.038	1.040	1.049	1.068	1.118	1.025	1.047	1.054	1.077

	Number concentration bias factor, PC measurements									
Component	$d \geq 1$ µm	$d \geq 2$ µm	$d \geq 3$ µm	$d \geq 5$ µm	$d \geq 7$ µm	$d \geq 10$ µm	$d \geq 15$ µm	$d \geq 20$ µm	$d \geq 25$ µm	$d \geq 30$ µm
RM vial/(2.5×, 5× vial) ratio	1.022	1.022	1.019	1.011	1.009	1.015	1.025	1.047	1.054	1.077
C_N	1.022	1.022	1.019	1.011	1.009	1.015	1.025	1.047	1.054	1.077

Appendix C: Summary Uncertainty Tables for Morphology Parameters

Tables 12 through 14 give a summary of the uncertainties associated with SEM, SFM, and PC morphology measurements, respectively. The uncertainties in aspect ratio, ellipse ratio, and compactness over various size bins are shown as well as the type of uncertainty (Type A or Type B). Type A uncertainties are those determined by statistical methods: Type B uncertainties are determined by non-statistical methods [15]. The dominant uncertainty (labeled "image analysis bias") arises for the optical images from the uncertainty of the diffraction correction delta or for the SEM images from the difference between hand-drawn and computer analysis of the morphology. An additional uncertainty arises from extraneous or background particles. It is not sufficient to simply count the background particles. If the morphology of the background particles exactly mimicked the ETFE morphology, for example, the background particles would have no impact on the measured parameter values for ETFE. For the SFM and PC, to assess this component of uncertainty, we analyzed the morphology parameters for both a regular data run and then for an artificial data run that had the background particles added in to the regular data run with no increase in the stated run volume. The difference in morphology parameters was taken as the standard uncertainty due to background particles. The repeatability is equal to the pooled ESDM of the measurements and is a small component of the uncertainty.

Table 12. Summary of morphology-parameter uncertainties for SEM measurements, expressed as standard uncertainties, u_c.

Component	Type	Aspect ratio uncertainty				
		$1 \leq d/\mu m < 1.5$	$1.5 \leq d/\mu m < 2$	$2 \leq d/\mu m < 3$	$3 \leq d/\mu m < 4$	$4 \leq d/\mu m < 8$
Repeatability	A	0.010	0.013	0.014	0.016	0.015
Background	B	0.017	0.017	0.017	0.017	0.017
Image analysis bias	B	0.066	0.057	0.051	0.042	0.039
$u_c(f_{asp})$		0.069	0.061	0.056	0.048	0.045
		Ellipse ratio uncertainty				
Repeatability	A	0.010	0.013	0.014	0.016	0.015
Background	B	0.017	0.017	0.017	0.017	0.017
Image analysis bias	B	0.039	0.034	0.030	0.022	0.022
$u_c(f_{ell})$		0.043	0.040	0.037	0.032	0.032
		Compactness uncertainty				
Repeatability	A	0.005	0.007	0.009	0.009	0.009
Background	B	0.012	0.012	0.012	0.012	0.012
Image analysis bias	B	0.044	0.035	0.030	0.028	0.028
$u_c(f_{comp})$		0.046	0.038	0.034	0.031	0.031

Table 13. Summary of morphology-parameter uncertainties for SFM measurements, expressed as standard uncertainties, u_c.

		Aspect ratio uncertainty						
Component	Type	$1 \leq d/\mu m < 1.5$	$1.5 \leq d/\mu m < 2$	$2 \leq d/\mu m < 3$	$3 \leq d/\mu m < 5$	$5 \leq d/\mu m < 10$	$10 \leq d/\mu m < 15$	$15 \leq d/\mu m < 50$
Repeatability	A	0.003	0.004	0.003	0.003	0.003	0.005	0.006
Background	B	0.001	0.002	0.001	0.001	0.000	0.000	0.000
Image analysis bias	B	0.068	0.058	0.050	0.039	0.030	0.026	0.024
$u_c(f_{asp})$		0.068	0.059	0.050	0.039	0.030	0.026	0.024
		Ellipse ratio uncertainty						
Repeatability	A	0.003	0.004	0.003	0.003	0.003	0.005	0.006
Background	B	0.003	0.002	0.002	0.002	0.000	0.000	0.000
Image analysis bias	B	0.086	0.074	0.063	0.050	0.038	0.032	0.030
$u_c(f_{ell})$		0.086	0.074	0.063	0.050	0.038	0.033	0.030
		Compactness uncertainty						
Repeatability	A	0.002	0.002	0.002	0.002	0.002	0.004	0.004
Background	B	0.001	0.001	0.001	0.001	0.000	0.000	0.000
Image analysis bias	B	0.064	0.055	0.046	0.036	0.029	0.025	0.024
$u_c(f_{comp})$		0.064	0.055	0.046	0.037	0.029	0.026	0.024

Table 14. Summary of morphology-parameter uncertainties for PC measurements, expressed as standard uncertainties, u_c.

Component	Type	Aspect ratio uncertainty					
		$1 \leq d/\mu m < 1.5$	$1.5 \leq d/\mu m < 2$	$2 \leq d/\mu m < 3$	$3 \leq d/\mu m < 5$	$5 \leq d/\mu m < 10$	$10 \leq d/\mu m < 25$
Repeatability	A	0.003	0.004	0.003	0.003	0.003	0.005
Background	B	0.002	0.001	0.001	0.001	0.001	0.001
Image analysis bias	B	0.072	0.060	0.050	0.040	0.031	0.025
$u_c(f_{asp})$		0.072	0.060	0.050	0.040	0.031	0.025
		Ellipse ratio uncertainty					
Repeatability	A	0.003	0.004	0.003	0.003	0.003	0.005
Background	B	0.004	0.004	0.002	0.002	0.001	0.001
Image analysis bias	B	0.090	0.075	0.064	0.051	0.039	0.031
$u_c(f_{ell})$		0.090	0.076	0.064	0.051	0.039	0.032
		Compactness uncertainty					
Repeatability	A	0.002	0.002	0.002	0.002	0.002	0.004
Background	B	0.017	0.004	0.003	0.001	0.001	0.001
Image analysis bias	B	0.067	0.055	0.047	0.037	0.030	0.025
$u_c(f_{comp})$		0.069	0.056	0.047	0.037	0.030	0.025